UNIVERSIDAD POLITECNICA DE VALENCIA

DEPARTAMENTO DE COMUNICACIONES

Máster Universitario en Tecnologías, Sistemas y Redes de Comunicaciones

Long fiber Bragg grating sensor interrogation

Autor: Amelia Lavinia Ricchiuti

Director: Salvador Sales Maicas

Fecha de comienzo: 15/09/2012

Lugar de trabajo: Grupo de Comunicaciones Ópticas y Cuánticas del iTEAM

Objetivos — El principal objetivo de este trabajo ha sido el estudio y desarrollo, tanto teórico como experimental, de sistemas novedosos para la interrogación de sensores de nivel de líquido y de temperatura basados en fibras ópticas de Bragg (FBGs) de alta reflectividad y en técnicas de Microwave Photonics (MWP).

Metodología — Durante el desarrollo de este trabajo han sido utilizadas dos técnicas diferentes para interrogar las FBGs. En ambos casos, el dispositivo que se ha utilizado para el sensado es una fibra de Bragg "fuerte" de una longitud de 10 cm. La primera metodología desarrollada, se basa en el uso de pulsos temporalmente estrechos (20-ps) que vienen reflejados por la FBG (el primer pulso se refleja al principio de la FBG y el segundo donde se produce un cambio de temperatura en la fibra) y capturados por un osciloscopio. La diferencia temporal entre los dos pulsos está relacionada con el nivel de líquido. La segunda metodología utilizada se basa en el uso de filtros de MWP y en el análisis de sus funciones de trasferencia, las cuales presentan cambios cuando un punto caliente se posiciona a lo largo de la FBG.

Desarrollos teóricos realizados — El principal desarrollo teórico ha sido el estudio de las características fundamentales de los reflectores de Bragg (tipo de FBG, respuesta espectral en trasmisión y reflexión, sensibilidad a cambios de temperatura, respuesta impulsional,…) y de los aspectos relacionados a filtros ópticos de MWP. El estudio teórico ha sido además acompañado por simulaciones de los modelos desarrollados.

Desarrollo de prototipos y trabajo de laboratorio — Una vez asimilada la teoría sobre los reflectores de Bragg y las técnicas de interrogación, han sido realizados en laboratorio los montajes necesarios para adquirir los datos relativos a las medidas de nivel de líquido y de temperatura, basándose en las metodologías descritas previamente.

Resultados — Los resultados mostrados a lo largo del trabajo se basan principalmente en las medidas experimentales de las magnitudes que provocan un cambio en el espectro de la FBG (aumento/disminución del nivel de líquido que presenta una temperatura diferente a la del ambiente, presencia y posición de un punto caliente a lo largo de la FBG).

Líneas futuras — Los siguientes pasos pueden cubrir diferentes aspectos de los sensores desarrollados: mejoras de los procesos de medida (en termino de resolución espacial, precisión, coste,…), estudio de la influencia de la forma y la duración temporal de los pulsos en la resolución espacial del sistema y en la respuesta temporal del grating, profundización en el análisis relativo a las medidas de temperatura, desarrollo de un nuevo sistema capaz de revelar la presencia de diferentes puntos calientes que presenten la misma temperatura.

Publicaciones

- Presentación de la comunicación titulada: **Fiber-optic liquid level sensing by using a long fiber Bragg grating**, fue presentada por la alumna en ***Young Women in Optical Fibre Sensing Research Evening***, Padova (Italy) 7-9 Abril 2013.
- **Amelia L. Ricchiuti**, David Barrera, Koji Nonaka, Salvador Sales, *Fiber-optic liquid level sensor using a long fiber Bragg grating*, in the 5th European Workshop on Optical Fibre Sensors, Kracow (Poland) 19-22 May 2013. (ISBN: 9780819496348)
- **Amelia L. Ricchiuti**, David Barrera, Salvador Sales, Luc Thévenaz, José Capmany, *Long fiber Bragg grating sensor interrogation using discrete-time microwave photonic filtering techniques*, submitted to Optics Express, 2013.

Abstract — The work proposed has been focused on the study, design and performance evaluation of fiber Bragg grating to the aim of realizing distributed sensing devices able to discriminate both liquid level and temperature change. In the first part of this work, the time-frequency analysis of a 10 cm-long FBG and its potential applications for fiber liquid-level sensing is proposed and experimentally demonstrated. A short optical pulse is coupled into a strong FBG. By monitoring the back-reflected pulse by an oscilloscope a liquid-level sensing is achieved with a spatial resolution of 2 mm, determined by half the incident pulse duration, and with a long measurement range of 10 cm. The temperature of the liquid can also be detected. In the second part of the work, a novel technique for interrogating photonic sensors based on long FBGs is presented and demonstrated, dedicated to detect the presence and the precise location of several spot events. The principle of operation is based on a technique used to analyze MWP filters. The long FBGs are used as quasi-distributed sensors. Several hot-spots can be detected along the FBG with a spatial resolution under 0.5 mm using a modulator and a photo-detector with a modest bandwidth of less than 1 GHz.

Autor: Amelia Lavinia Ricchiuti, email: amric1@iteam.upv.es
Director: Salvador Sales Maicas, email: ssales@dcom.upv.es
Fecha de entrega: 09-09-13

CONTENTS

I. Introduction

The discovery and development of fiber optic technology has had an immeasurable impact on the technological and scientific world. Over the past four decades, fiber optics have been applied in many different fields, including the medical field, the military, industry, networking, and communication systems. Although the field of fiber optics itself is very broad, one of the largest contributions it has made is in the world of telecommunication where they made possible high-quality, high capacity and long distance links. In addition to application in telecommunications, fiber optics are also largely utilized in the growing field of fiber sensing systems. The reason for this choice is largely due to the characteristics and properties of optical fibers; indeed, optical fiber sensors are made of dielectric material and therefore they are non-conducting, immune to electromagnetic interference, chemically inert and spark free [1].

Despite the advancements in optical fiber manufacturing, basic optical components like mirrors, reflectors and wavelength filters have been a challenge to integrate with optical fibers. However, all these changed with the discovery of the possibility to alter the core index of refraction in a single mode optical fiber by optical absorption of UV light. This photosensitivity of optical fibers allows a permanent periodic or aperiodic change in the refraction index of the core of the optical fiber, which is known as *fiber Bragg grating*. Fiber Bragg gratings (FBGs) result to be a key components in optical and communication systems since they are able to perform many primary functions, such as reflection and filtering, in a highly efficient, low loss manner. This ability has been used to stimulated a number of significant innovations [2].

I.1. *Fundamentals of fiber Bragg gratings*

Fiber Bragg gratings are considered key components in all-fiber based systems due to their characteristics such as simplicity, compatibility, polarization independence and low cost. An FBG is an optical component characterized by a periodic or aperiodic perturbation of the effective refractive index in the core of an optical fiber, which is permanently photo-induced along the length of a single mode fiber (SMF). A schematic representation of a Bragg grating inscribed into the core of an optical fiber is shown in Fig. 1. This type of uniform fiber grating, where the phase fronts are perpendicular to the fiber's longitudinal axis with grating planes having a constant period, is considered the fundamental building blocks for most Bragg grating structures.

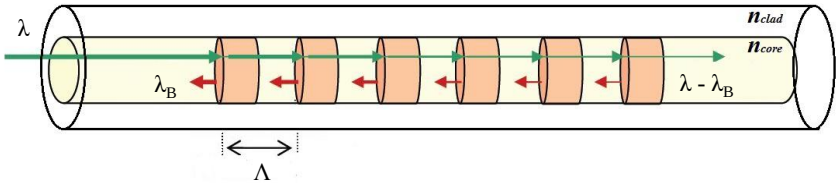

Fig. 1. Schematic representation of a Bragg grating.

Light guided along the core of the FBG is scattered by each grating plane and in case the Bragg condition is not satisfied, the reflected light from each of the subsequent planes becomes progressively out of phase and so is cancelled out. Furthermore, light at wavelength that is different with the Bragg wavelength, experiences a very weak reflection at each of the planes because of the index mismatch; this reflection accumulates over the length of the grating. Where the Bragg condition is satisfied the contributions of reflected light from each grating plane add constructively in the backward direction to form a back-reflected peak with a center wavelength defined by the grating parameters.

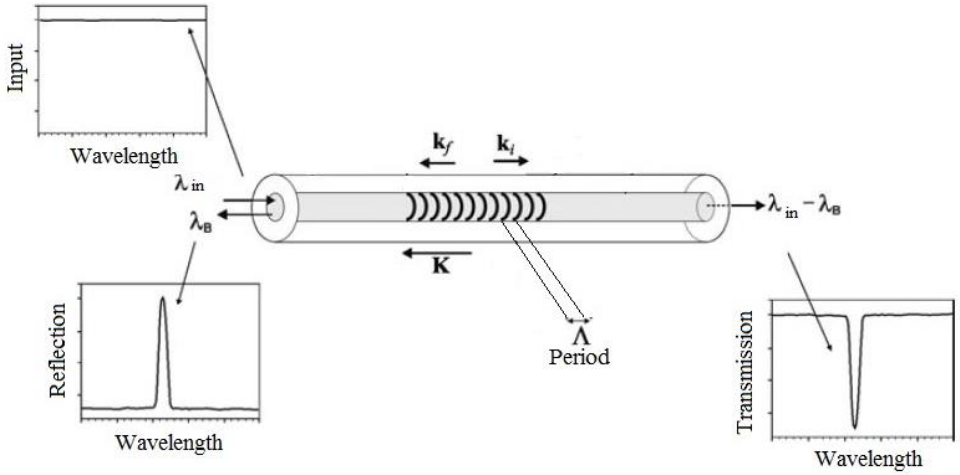

Fig. 2. Schematic representation of a uniform Bragg grating. Also shown are the incident, scattered and grating wavevectors.

Figure 2 shows a schematic of a uniform Bragg grating with constant index of modulation amplitude and period. Since the Bragg grating condition is fulfilled, this requirement satisfies both energy and momentum conservation. Energy conservation implies that the frequency of the incident radiation and the reflected radiation is the same, while momentum conservation requires that the wavevector of the incident wave, k_i, plus the grating wavevector, K, equal the wavevector of the scattered radiation k_f, as expressed in the Eq. 1:

$$k_i + K = k_f \tag{1}$$

where the grating wavevector, K, has a magnitude $2\pi/\Lambda$ (Λ is the grating period shown in Fig. 2) and a direction normal to the grating planes. The wavevector of the scattered radiation is equal in magnitude, but opposite in direction, to the wavevector of the incident wave. In this way, the momentum conservation condition becomes:

$$2\left(\frac{2\pi n_{eff}}{\lambda_{\mathbf{B}}}\right) = \frac{2\pi}{\Lambda} \tag{2}$$

which can be simplified to the *first order Bragg condition*:

$$\lambda_B = 2\Lambda n_{eff} \tag{3}$$

where the Bragg grating wavelength, λ_B, corresponds to the free space center wavelength of the input light that will be back-reflected from the grating, and n_{eff} is the effective refractive index of the core at the free space center wavelength.

I.2. *Uniform fiber Bragg gratings*

For a uniform Bragg grating having an average refractive index, n_0, the index of the refractive profile along the fiber longitudinal axis, z, can be expressed as:

$$n(z) = n_0 + \Delta n \cdot \cos\left(\frac{2\pi z}{\Lambda}\right) \tag{4}$$

where Δn is the amplitude of the refractive index perturbation, which typically varies between 10^{-5} (for weak FBG) and 10^{-3} (for strong FBG). By means of the *coupled-mode theory* [3] the reflectivity of a uniform Bragg grating with constant modulation amplitude and period is given by:

$$R(l,\lambda) = \frac{\kappa^2 \sinh^2(sl)}{\Delta\beta^2 \sinh^2(sl) + s^2 \cosh^2(sl)} \tag{5}$$

The reflectivity of the grating, $R(l,\lambda)$, is a function of the grating length l and the wavelength λ. κ is the coupling coefficient, $\beta = 2\pi n_0/\lambda$ is the propagation constant, $\Delta\beta = \beta - \pi/\Lambda$ is the detuning wavevector and $s^2 = \kappa^2 - \Delta\beta^2$. If the index perturbation experiences a sinusoidal variation, the coupling coefficient is given by:

$$\kappa = \frac{\pi\Delta n}{\lambda} M_{power} \tag{6}$$

where M_{power} is the fraction of the fiber mode power contained by the fiber core. At the center wavelength of the grating the wavevector detuning is $\Delta\beta = 0$, and the reflectivity becomes:

$$R(l,\lambda) = \tanh^2(\kappa l) \tag{7}$$

According to Eq. 7, the grating reflectivity increases as the induced index of refraction change gets larger and as the length of the grating increases. Fig. 3 shows the reflection spectrum of a uniform Bragg grating as a function of the wavelength, when the length is of 1 cm and a coupling coefficient of 0.25 mm^{-1}. The lateral lobes are due to multiple reflections to and from opposite ends of the grating region and the sinc shape of the reflection spectrum arises mathematically through

the Fourier transform of a finite harmonic signal, while an infinitely long grating would transform into an ideal delta function response in the frequency domain.

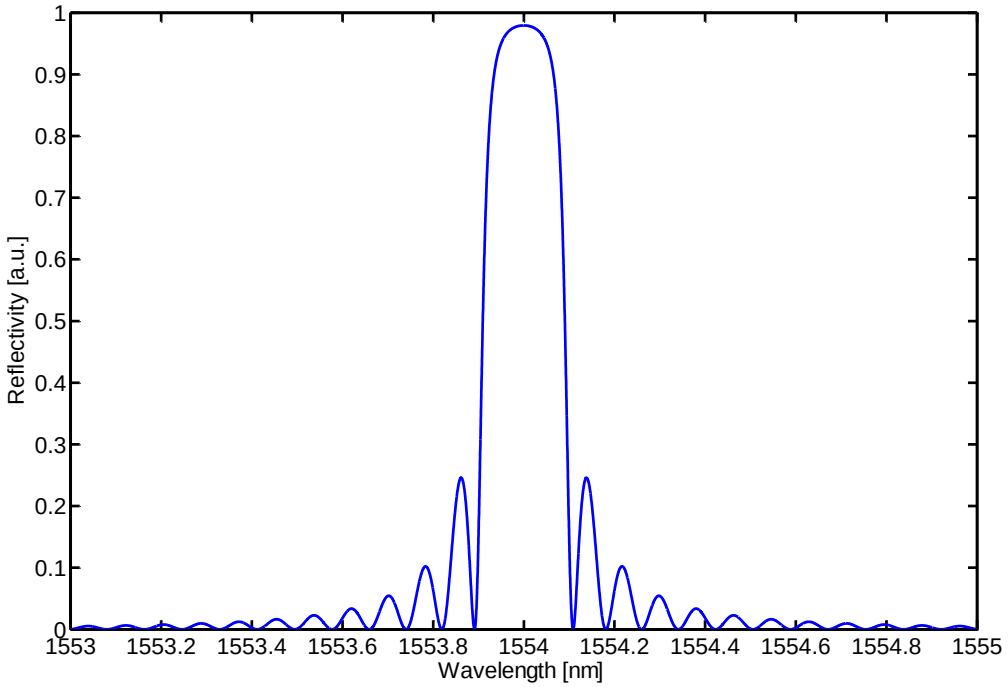

Fig. 3. Typical reflection spectrum of a uniform Bragg grating.

Finally, a general expression for estimating the full-width-half maximum (FWHM) bandwidth of the Bragg grating is given by [4]:

$$\Delta\lambda = \lambda_B S \sqrt{\left(\frac{\Delta n}{2n_0}\right)^2 + \left(\frac{1}{N}\right)^2} \tag{8}$$

where N is the number of the grating planes and S is a parameter that is close to the unit whilst the FBG is strong and $S \approx 0.5$ for a weak FBG. Therefore, a strong grating typically has a FWHM bandwidth larger than a weak grating refractive index of the core at the free space center wavelength.

I.3. *Weak and strong FBGs analysis*

Bragg gratings grow differently in response to particular inscription conditions and its strength can be controlled by the ultraviolet exposure time during the fabrication process. A set of simulations were performed in order to analyze the behavior of four different FBGs. Fig. 4 illustrates the reflection spectra of four Bragg grating as a function of the wavelength. All the gratings have a length of $l = 1\ cm$, and a Bragg wavelength resonance of $\lambda_B = 1554\ nm$, while the grating strengths are different. Indeed, the amplitudes of the refractive index perturbation are $\Delta n_1 = 3 \cdot 10^{-5}$ (weak

FBG), $\Delta n_2 = 8 \cdot 10^{-5}$ (medium FBG), $\Delta n_3 = 3 \cdot 10^{-4}$ (strong FBG) and $\Delta n_4 = 10^{-3}$ (very strong FBG). As shown in Fig. 4 and according to Eq. 8, the FWHM bandwidth of the grating increases as the FBG gets stronger.

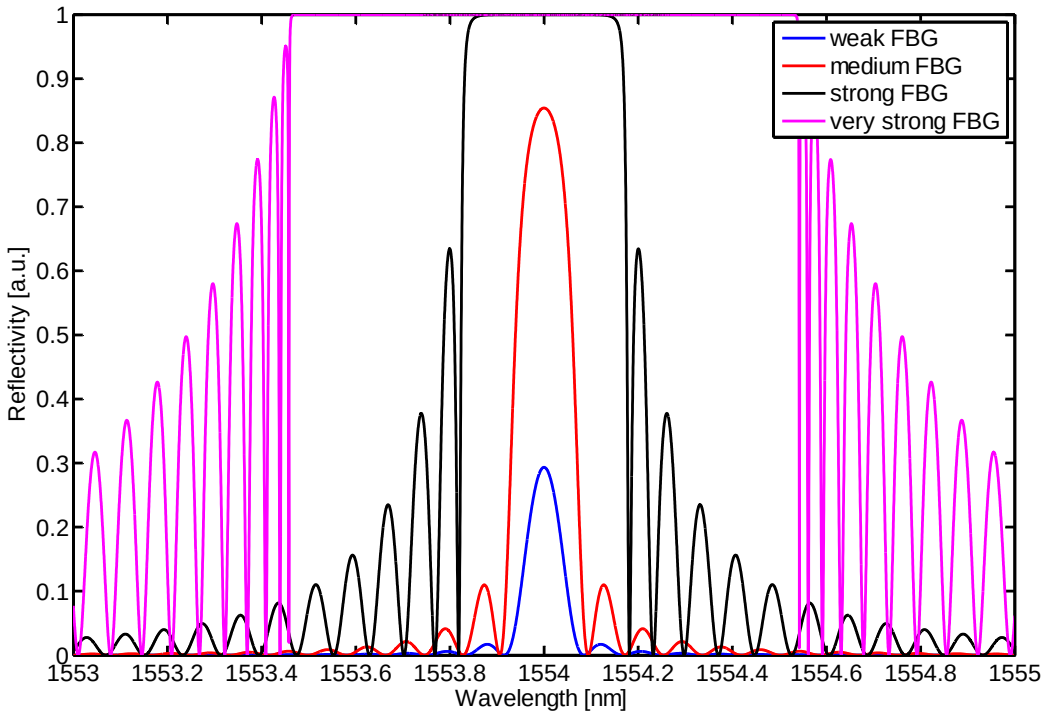

Fig. 4. Reflectivity response of four grating having same length but different strengths: $\Delta n_1 = 3 \cdot 10^{-5}$ (weak), $\Delta n_2 = 8 \cdot 10^{-5}$ (medium), $\Delta n_3 = 3 \cdot 10^{-4}$ (strong), $\Delta n_4 = 10^{-3}$ (very strong).

Another set of simulations was performed with the aim of studying the interaction between a short broadband optical pulse and the four fiber gratings mentioned before. Specifically, the theoretical analysis of linear pulse propagation through uniform FBGs for the case in which the input pulse spectrum is broader than that of the grating response, was investigated [5]. According to the mathematical modeling point of view, the reflected pulse from the grating is the *Inverse Fourier Transform* (IFT) of the product between the input Gaussian pulse spectrum and the grating reflection response.

A symmetric 20-ps Gaussian pulse is assumed as the short input signal and the reflected pulses from the different gratings, varying in strength from weak to very strong, are illustrated in Fig. 5. As the grating strength increases, it is possible to observe a separation of the reflected pulse into two distinct components: a main reflection peak and transient sub-pulses. In particular, the main reflection peak and the start of the transient sub-pulses are separated in time by the round-trip propagation time through the Bragg grating. Furthermore, both the duration and the number of the oscillations in the transient sub-pulses increase with increasing grating strength. Finally, Fig. 5 shows as in the case of weak FBG (Fig. 5a), the incident pulse is continuously back-reflected while

propagating through the entire grating length, while in the case of strong FBG (Fig. 5c and Fig. 5d), the incident pulse is almost completely reflected in the initial section of the grating.

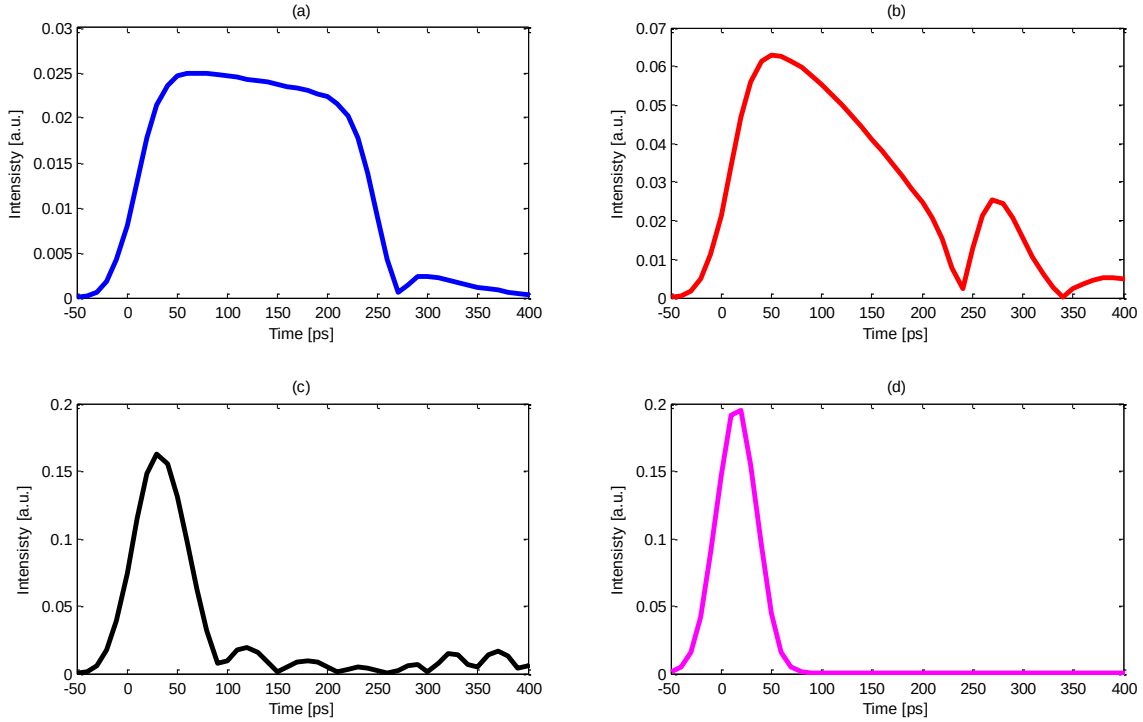

Fig. 5. Reflected pulses from uniform FBGs of length l=1 cm and different grating strengths: a) $\Delta n_1=3\cdot10^{-5}$, b) $\Delta n_2=8\cdot10^{-5}$, c) $\Delta n_3=3\cdot10^{-4}$, d) $\Delta n_4=10^{-3}$. The input is a 20-ps Gaussian pulse.

I.4. *Strain and temperature sensitivity of FBGs*

As mentioned before, the Bragg grating resonance, which is the center wavelength of the back-reflected light from an FBG, depends on the effective refractive index and the periodicity of the grating. Moreover, the effective refractive index, as well as the periodic spacing between the grating planes, will be affected by strain and temperature changes. By deriving the Eq. 3 as a function of the longitudinal deformation and the temperature, the equation that define the behavior of the Bragg grating as sensor is obtained:

$$\Delta\lambda_B = \frac{\partial\lambda_B}{\partial\varepsilon}\varepsilon + \frac{\partial\lambda_B}{\partial T}\Delta T \tag{9}$$

$$\Delta\lambda_B = 2\left[\left(\frac{\partial n_{eff}}{\partial l}\Lambda + n_{eff}\frac{\partial\Lambda}{\partial l}\right)\Delta l + \left(\frac{\partial n_{eff}}{\partial T}\Lambda + n_{eff}\frac{\partial\Lambda}{\partial T}\right)\Delta T\right] \tag{10}$$

where ε is the unitary deformation applied to the fiber sensor, Δl is the strain change and ΔT is the temperature change. Thus, the first term in Eq.10 represents the strain effect on an optical fiber,

which corresponds to a change in the grating spacing and the strain-optic induced change in the refractive index. This strain effect term can be expressed as [6]:

$$\Delta\lambda_B = \lambda_B\left[1-\frac{n^2}{2}\left[p_{12}-\nu\left(p_{11}+p_{12}\right)\right]\right]\varepsilon_z \tag{11}$$

where p_{11} and p_{12} are the strain optic tensor components, ν is the Poisson's ratio and $\varepsilon_z = \delta l/l$.

The second term in Eq. 10 represents the effect of temperature on the grating. A shift in the Bragg wavelength due to thermal expansion changes the grating period Λ and then the refractive index. This fractional wavelength shift for a temperature change ΔT can be written as [6]:

$$\Delta\lambda_B = \lambda_B(\alpha_\Lambda + \alpha_n)\Delta T \tag{12}$$

where $\alpha_\Lambda = (1/\Lambda)(\partial\Lambda/\partial T)$ represents the thermal expansion coefficient and $\alpha_n = (1/n)(\partial n/\partial T)$ is the thermo-optic coefficient. To conclude, due to the strain and temperature dependence of the Bragg grating parameters n and Λ, the wavelength of the reflected component will also change in function of temperature and/or strain, as shown in Fig. 6, making the FBGs able to work as strain and/or temperature sensors.

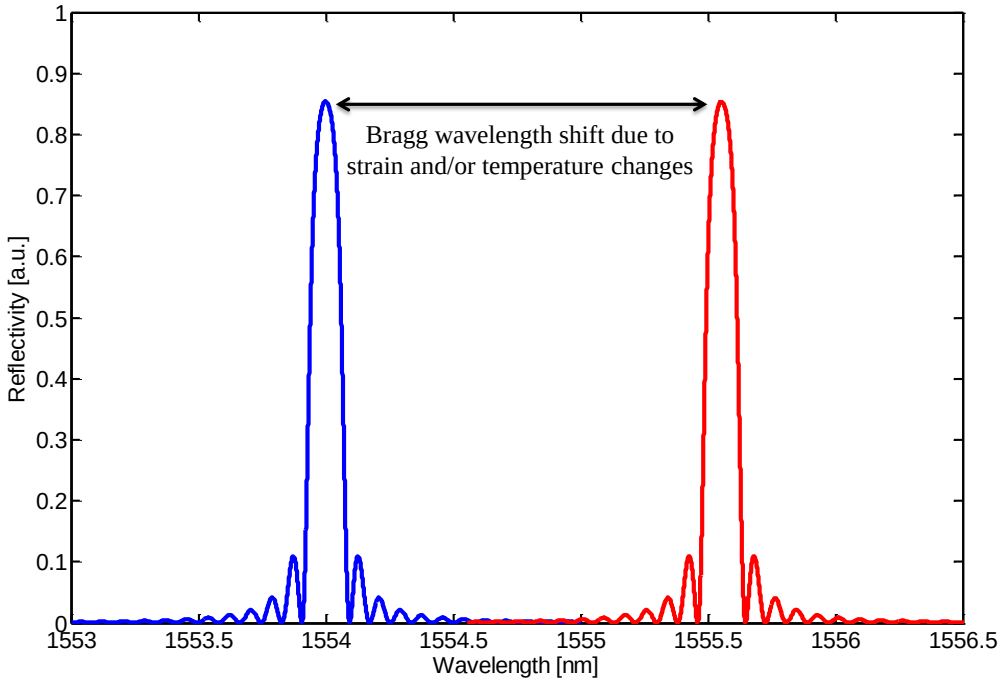

Fig. 6. Bragg wavelength shift in a FBG under temperature and/or strain changes.

I.5. *Grating-length dependence*

The spectral response of a Bragg grating is affected as the length of the grating is altered. Fig. 7 shows the spectral profile of three uniform Bragg gratings, having the same value of the amplitude

of the refractive index perturbation, $\Delta n_1 = 3 \cdot 10^{-5}$ and different length (1, 3 and 10 cm). The various plots clearly demonstrate that the reflectivity increases with increasing length. Indeed, the 1 cm long uniform grating shows a reflectivity of approximately 0.3, which is referred as a weak FBG, that of the 3 cm long grating is approximately 0.9, which is referred as a medium FBG and finally the 10 cm-long grating exhibits a reflectivity of 100% which is referred as a strong FBG.

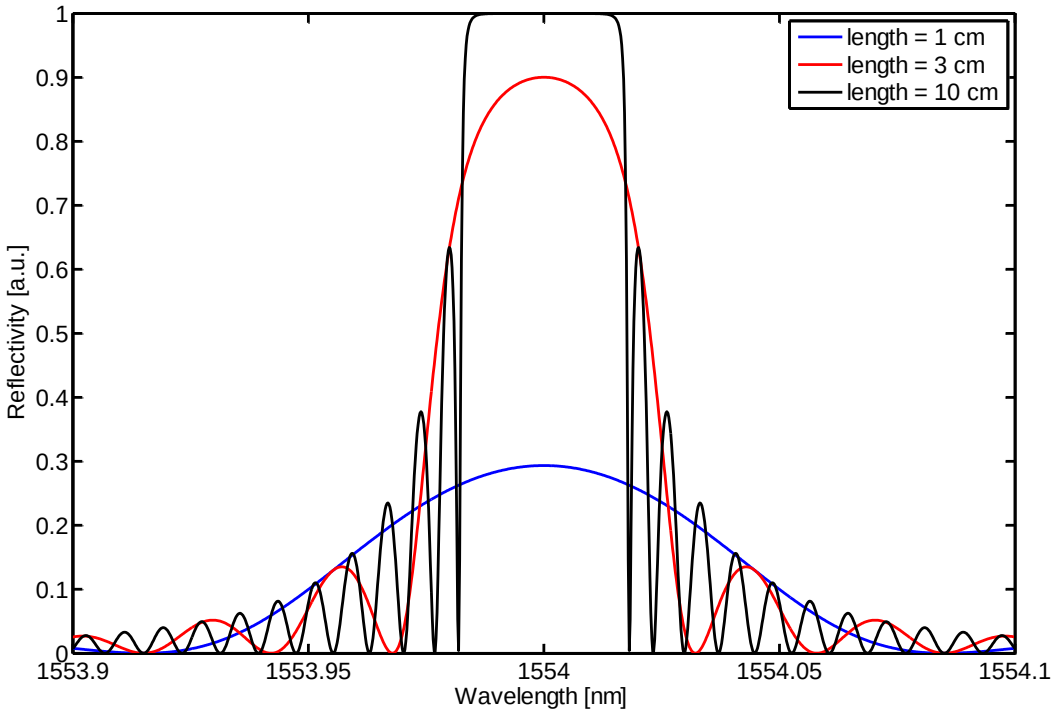

Fig. 7. Spectral reflectivity response from uniform Bragg gratings having same amplitude of the refractive index perturbation and different lengths.

Furthermore, Fig. 7 demonstrates that the bandwidth of the gratings decreases with increasing length. Theoretically FBGs may be fabricated with extremely small bandwidths by simply increasing the grating length. However, practically Bragg gratings are not easy to manufacture; in fact the error associated with the spacing between the periods of a grating during fabrication process is cumulative, which means that with increasing grating length the total error increases, resulting in out-of-phase periods and leading to broadening of the Bragg grating reflection spectrum. Furthermore, if a long perfect Bragg grating is fabricated, the effects of the environment have to be considered very carefully. For example, any temperature and/or strain variation on the grating will cause the periods to move out of phase resulting in broadening of the Bragg grating reflection [2].

II. Liquid-level and temperature sensor using long FBGs

Liquid level sensing is an indispensable requirement in many applications in which monitoring of the liquid's volume is necessary, for example in chemical processing, fuel storage and transportation. Electrical liquid-level sensors are widely used in practice, but their applicability, reliability, and safety is compromised if the liquid to be monitored is conductive or corrosive or if the environment is potentially explosive. Moreover, in case of multiple sensors, an electrical liquid-level sensing system requires intensive cabling and feed-through, unavoidably increasing the system cost and complexity.

Optical fiber liquid-level sensors offer many advantages under these rigorous conditions because they are made of dielectric material and thus they are no-conducting and anti-corrosive. Furthermore, they are immune to electromagnetic interference chemically inert and spark free. Another important characteristic of fiber optic sensors is their multiplexing capability, which enables one to use a shared light source and detection system for multipoint measurement, thanks to various fiber-optic components developed for communications [1].

Different kinds of liquid-level sensing techniques have been reported; for example using long-period gratings (LPGs) in which refractive-index sensitivity is used to measure the length of a fiber immersed in a liquid [7]. The liquid level can also be determined using a FBG etched to enhance the sensitivity to the refractive index of the liquid [8], or by using mechanical components that are able to induce expansion or compression in the fiber which induce change in transmission or reflection response [9], [10]. Another kind of liquid-level sensor is based on multimode interference (MMI) effects by using a no-core multimode fiber (MMF) and detecting shift in the spectral response [11]. Optical energy carried in the optical fiber can be used to heat in-fiber in order to alter the optical response to the surrounding media [12]. In [13] is proposed an intensity-based fiber-optic liquid-level gauge based on the principle of the total internal reflection (TIR) and on the optical attenuation in a fiber where the liquid acted as a second cladding. The principle of TIR is also used in [14], where a tip-shaped probe is used and the intensity of the back-reflected light decreases when the tip is dipped in the liquid. In [15] is presented a lateral side-polished fiber optic liquid-level sensor based on the serial connection of liquid probe where the change in the transmission response of the plastic optical fiber (POF) is detected.

In this chapter, a technique for fiber-optic liquid-level sensors based on a 10 cm-long uniform FBG is proposed and demonstrated. Uniform FBGs are simple to fabricate and to interrogate. Besides, FBGs can be multiplexed easily for multipoint measurements and the fluctuations of the received power do not affect the measurements. A short optical pulse having a duration much shorter than the transit time through the FBG has been employed. If a portion of the FBG is immersed in a liquid having a temperature different to the surrounding ambient, the structure of the uniform grating is distorted and its response will change. By capturing and monitoring the reflected

pulse by means of an oscilloscope, it is possible to implement a liquid-level sensor with a high resolution and long measurement range based on a simple layout. The temperature of the liquid can also be measured.

II.1. *Principle of operation*

The operation principle to analyze the long FBGs spectral properties relays on optical time-domain reflectometry (OTDR) [16], is illustrated in Fig. 8. An short optical pulse, which has a duration much shorter than the transit time through the FBG, is launched into the long grating. Thus, if the grating reflectivity is enough, the incident is almost completely reflected in the initial section of the grating (Fig. 8a).

If an external perturbation (i.e. strain or temperature change) is induced in any part of the grating, a change in the structure of this section of the FBG is expected. Indeed, it can be considered to have two separate gratings; the first one centered at the Bragg wavelength of the original FBG and the other one centered at a new Bragg wavelength. In this case, when the input optical pulse is coupled into the FBG, a separation of the reflected pulse into two distinct components can be observed; a main reflection pulse will be reflected in the initial section of the first FBG, and a transient sub-pulse which will be reflected in the initial section of the second FBG (i. e. the portion under external perturbation). The main reflection pulse and the sub-pulse are separated in time by the round-trip propagation time between the two different gratings. By evaluating the time-separation between the two peaks, the position of the grating local perturbation can be detected.

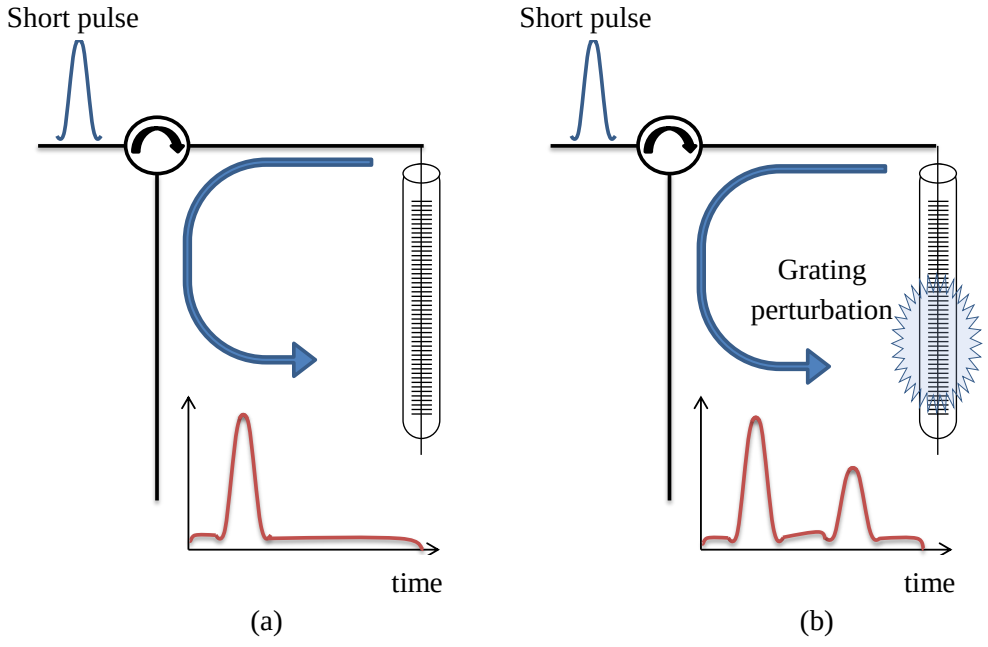

Fig. 8 a) and b). Operation principle to characterize the spectral properties of the Bragg gratings.

II.2. *Sensor system design and experiment*

As previously mentioned, in order to implement an FBG-based sensor, the coupling coefficient κ, which is defined as the optical power coupling between counter propagating modes per unit of length, has to be sufficiently high enough to ensure that the FBG reflection temporal impulse response is similar to the one illustrated in Fig. 8. In this experiment, a 10 cm-long FBG with high total reflectivity was employed. The nominal FBG spectrum is measured under CW illumination giving a FWHM spectral width of 11.25 GHz.

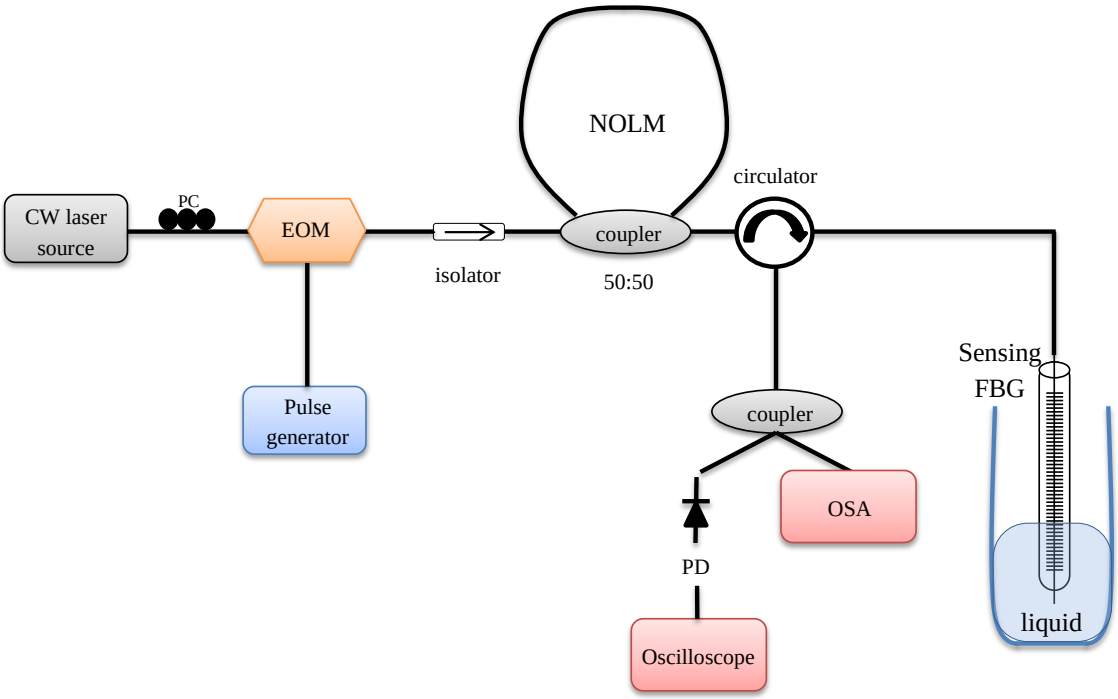

Fig. 9. Experimental layout to interrogate 10 cm-long sensing grating.

A schematic diagram of the proposed Bragg grating liquid-level and temperature sensor is shown in Fig. 9. A continuous wave (CW) laser source operating at 1553.9 nm is externally modulated by means of an electro-optical modulator (EOM) through a pulse train with 2 ns repetition rate, equivalent to a twice round-trip propagation distance through the grating (i.e. 40 cm). In this way, it is ensured that only one pulse travels along the FBG and any reflection overlapping between adjacent pulses is avoided. At the output of the EOM, the modulated signal is passed through an isolator and then coupled into an non-linear-optical loop mirror (NOLM) [17]. The aim of the NOLM is to comprise the optical pulse and suppress any stray background direct current (DC) component in order to avoid undesirables interference noise components possibly caused by CW reflections. Therefore, at the output of the NOLM, a 20-ps Gaussian pulse is obtained and then launched into the 10 cm sensing FBG by means of a circulator. The resonance of the Bragg grating is 1553.9 nm at room temperature. The FBG is mounted inside a graduated

container. During the experiment, the container is filled (or emptied) with water which has a temperature higher than the surrounding ambient. Finally, the reflected pulse is captured and monitored by using an Optical Signal Analyzer (OSA) and an oscilloscope.

The measurement system is based on the measurement of the central frequency distribution of the FBG based on time- frequency domain analysis. When the short optical pulse is launched into the fiber under test, as the grating is strong, the incident pulse is almost completely reflected in the initial section of the grating [5].

As it was mentioned before, when the FBG is partially immersed within the liquid having a higher temperature than the surrounding ambient, the structure of the section of the grating immersed will change. Indeed, it can be considered to have two separate gratings; the first one centered at the Bragg wavelength of the original FBG (1553.9 nm) and the other one centered at a new Bragg wavelength. In this case, when the input optical pulse is coupled into the FBG, a separation of the reflected pulse into two distinct components can be observed; a main reflection pulse will be reflected in the initial section of the first FBG, and a transient sub-pulse will be reflected in the initial section of the second FBG (i. e. the portion immersed in the liquid). The main reflection pulse and the sub-pulse are separated in time by the round-trip propagation time between the two different gratings. By evaluating the time-separation between the two peaks, the liquid level can be detected with high spatial resolution. Indeed, as the pulse is always reflected at the beginning of each one of the FBGs, the spatial resolution of this technique is essentially determined by half the pulse duration, such as OTDR technique. As the optical pulse has duration of 20-ps, the spatial resolution of this system is around 2 mm.

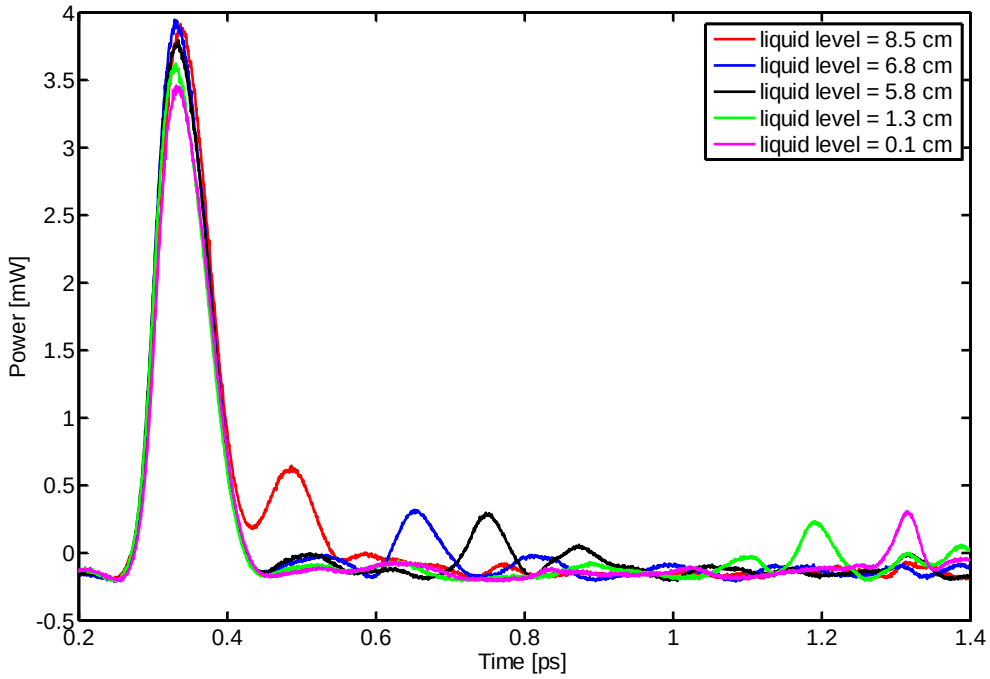

Fig.10. Measurements of the reflected pulse time waveform obtained by step-emptying the container.

Figure 10 shows a set of experimental measurements of the reflected pulse time waveform obtained by step-emptying the container. The values of the liquid level can be measured by means of the time difference between the first back-reflected pulse and the second one. Therefore, the liquid level L is detected by means of Eq.13, where $l = 10\ cm$ is the length of the FBG, Δt is the time separation between the main reflection pulse and the sub-pulse, c is the speed velocity in the vacuum and n is the fiber refractive index.

$$L = l - \frac{\Delta t \cdot c}{2n} \tag{13}$$

II.3. *System resolution*

As mentioned before, the operation principle to perform the liquid level measurements, relays on the OTDR. This opto-electronic technique used to characterize an optical fiber, is based on the principle that, when an optical pulse is injected onto the fiber, a small amount of the signal is continuously back-reflected by "irregularities" (splice, connectors ,fiber end,…). By measuring the arrival time of the returning light, the locations and amplitudes of these irregularities can be determined [16].

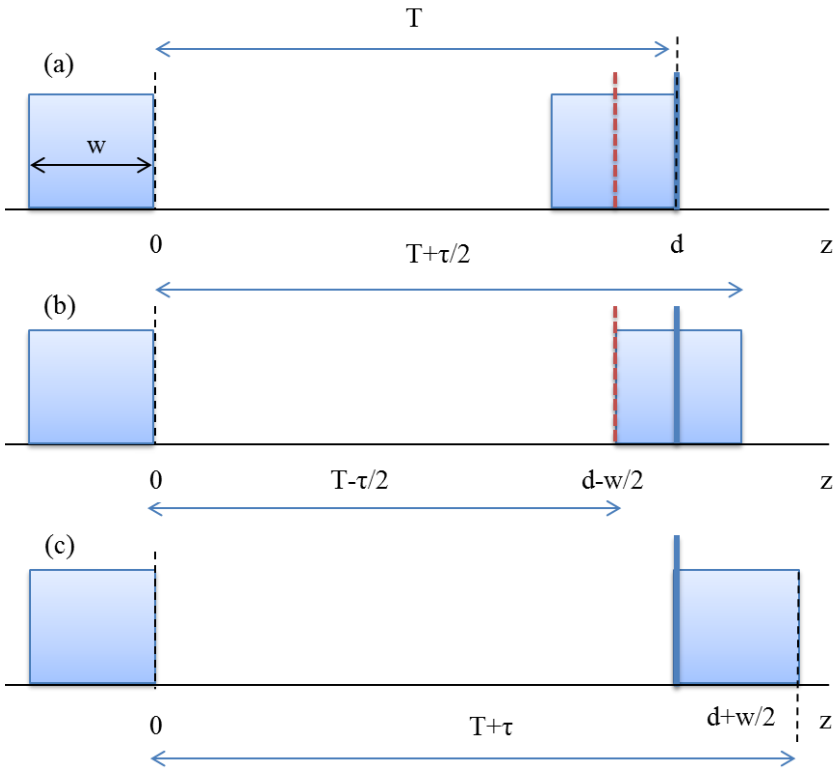

Fig. 11. Schematic illustration of the pulse propagation along the fiber, used to determine the spatial resolution of the system.

Figure 11a is schematically depicting the pulse travelling along the fiber. The pulse is extended along a longitudinal length $w = \tau v_g$, where τ is the pulse temporal duration and v_g represents the group velocity. A small amount of the pulse is back-reflected by the irregularity situated at $z = d$. At the instant $t = T$ the initial section of the optical pulse is reflected and the round-trip time will be equal to $t_{rt} = 2T$. In this way, at the instant $t = T+\tau$ the end of the pulse is reflected with a round-trip time $t_{rt} = 2(T+\tau/2)$, as illustrated in Fig.11c.

As the spatial resolution is defined as the minimum distance over which it is not possible to distinguish two events, if another irregularity is situated at a temporal distance $t \geq \tau/2$ far from the first irregularity, the two events result still distinguishable. On the contrary, when $t < \tau/2$ the back-reflected signals related to the two different events will be overlapped. Therefore, the system time resolution results in $\tau_{res} = \tau/2$, which means that for an optical pulse with duration of 20-ps, the spatial resolution of this system is around 2 mm. Finally, it is important to point out that it is possible to achieve a better spatial resolution by comprising the optical input pulse.

II.4. *Influence of the pulse time-duration*

As mentioned before, the system proposed allows to evaluate the liquid level by means of the time difference between the first back-reflected pulse and the second one. Furthermore, as it was explained in the previous section, pulse time-duration influences the spatial resolution of the method. Indeed, the spectral width of an optical pulse can be evaluated by means the Time-Bandwidth Product (TBP), which is defined as the product of the pulse temporal duration and spectral width. For the 20-ps Gaussian pulse, the spectral width results $FWHM \approx 0.441/20\ ps$ [3], i.e. $FWHM \approx 22\ GHz$, while the nominal FBG spectrum (measured under CW illumination) has a FWHM bandwidth of 11.25 GHz.

As the FWHM of the incident pulse is almost double that the FWHM of the FBG, when a change in the liquid level occurs and provokes a change in the FBG spectrum, the main reflection peak is still completely captured by the Gaussian pulse and then its amplitude remains fairly constant, while the shifted secondary peak is not totally captured thus its amplitude is considerably lower (see Fig.10). The other reason why the amplitude of the sub-pulse is largely lower than the amplitude of the main pulse is because the grating is very strong and then the most part of the incident pulse is back-reflected in the initial part of the FBG and just a small portion of the optical input pulse will travel along the remainder of the fiber.

In order to evaluate the influence of the time-duration of the optical pulse in this technique, numerical simulations have been implemented. Fig. 12 illustrates the product between the input pulse spectrum and the grating reflection response. It is assumed a grating reflection response of a 10 cm FBG with $FWHM \approx 11\ GHz$. Then, it is simulated that 4 cm of the grating is immersed in a liquid having temperature 35°C higher than the surrounding ambient. Finally the FBG spectrum is

multiplied with four different input pulse spectra, varying in temporal duration (20, 17, 10 and 4.5-ps). By analyzing these numerical simulations, it can be seen that using an optical input pulse of 20-ps, the maximum temperature variation detectable by the sensor is almost 35°C, as showed in Fig. 12(a). Nevertheless, if the time duration of the input pulse is reduced, i.e. the spectral response is enhanced, temperature variation higher than 35°C can also be measured.

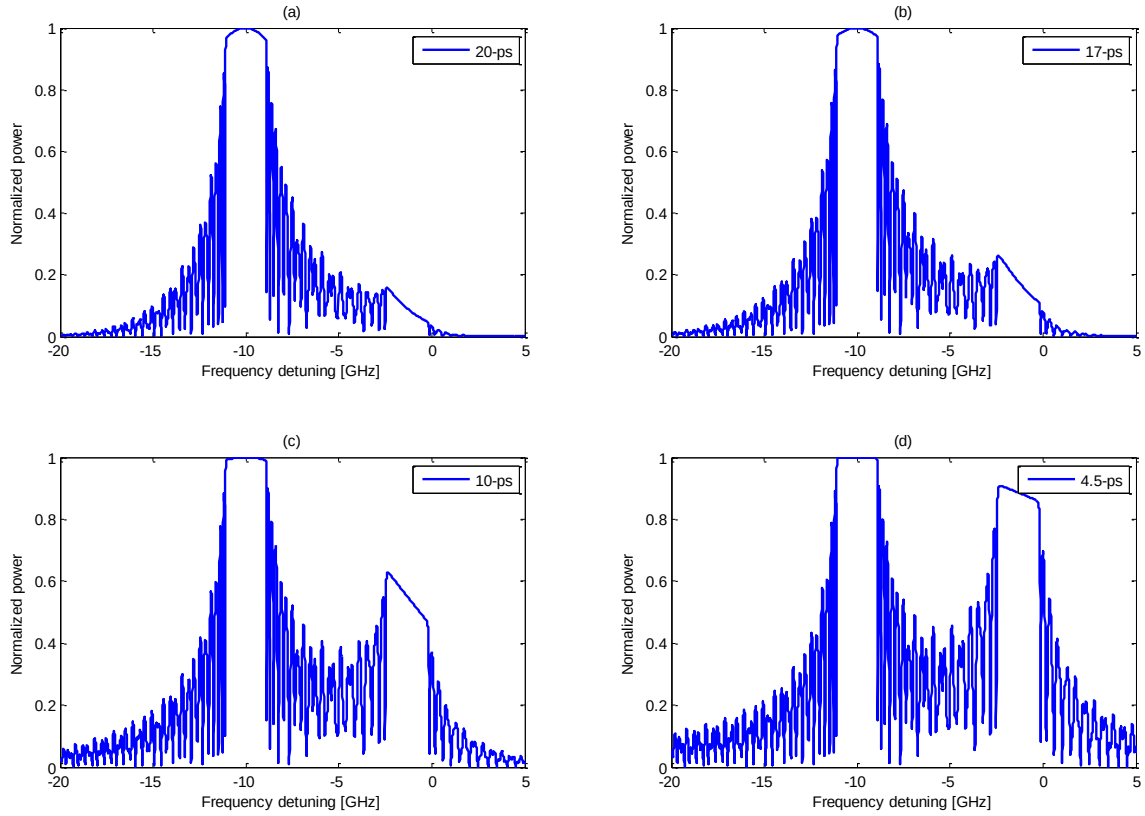

Fig. 12. Product between the grating reflection response of a 10 cm FBG with 11-GHz FWHM bandwidth when 4 cm of the grating is immersed in a liquid having temperature 35°C higher than the surrounding ambient and different input pulse spectrums. The values of time-duration of the optical pulse are 20-ps (a), 17-ps (b), 10-ps (c) and 4.5-ps (d).

According to the TBP theory, signals of short duration have wide spectral width and vice versa. This fact means that, if the optical input pulse is significantly compressed (as illustrated in Fig. 12c and Fig.12d) it is possible to achieve a higher spatial resolution and, as the related spectral response of the pulse is enhanced, it is also possible to measure high temperature changes. For this reason the previous measurements are repeated using a shorter input pulse, as illustrated in Fig. 13, where only the sub-pulses are depicted. In this case, as the optical input pulse has duration of 5-ps, the improved spatial resolution results 0.5mm.

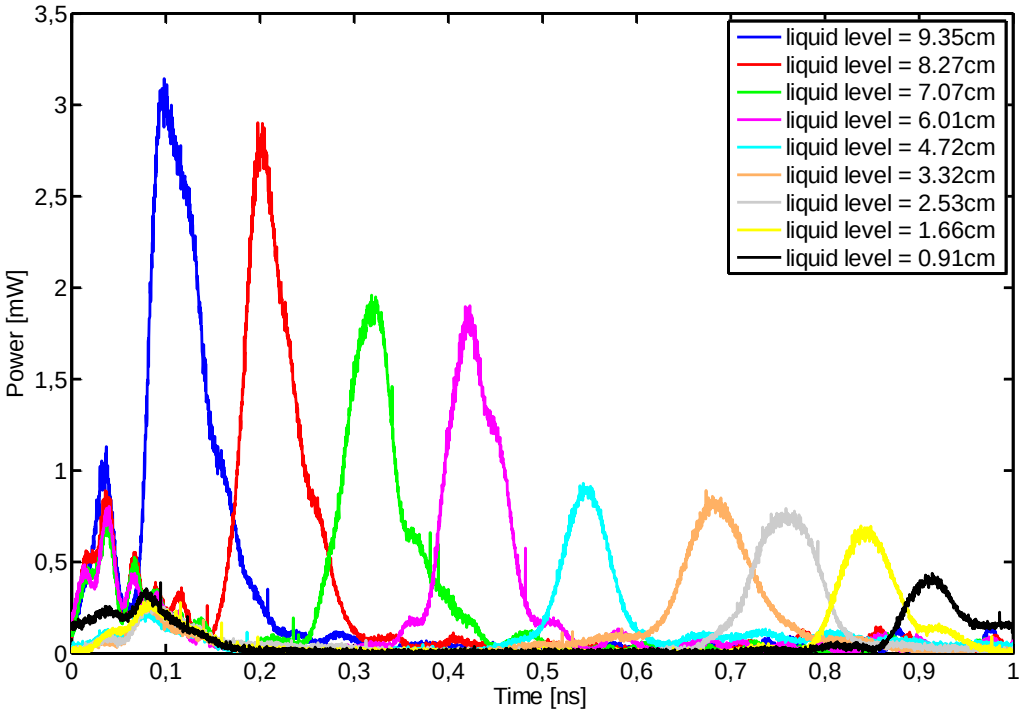

Fig.13. Measurements of the reflected sub-pulse time waveform, when a 5-ps Gaussian pulse is used as input signal.

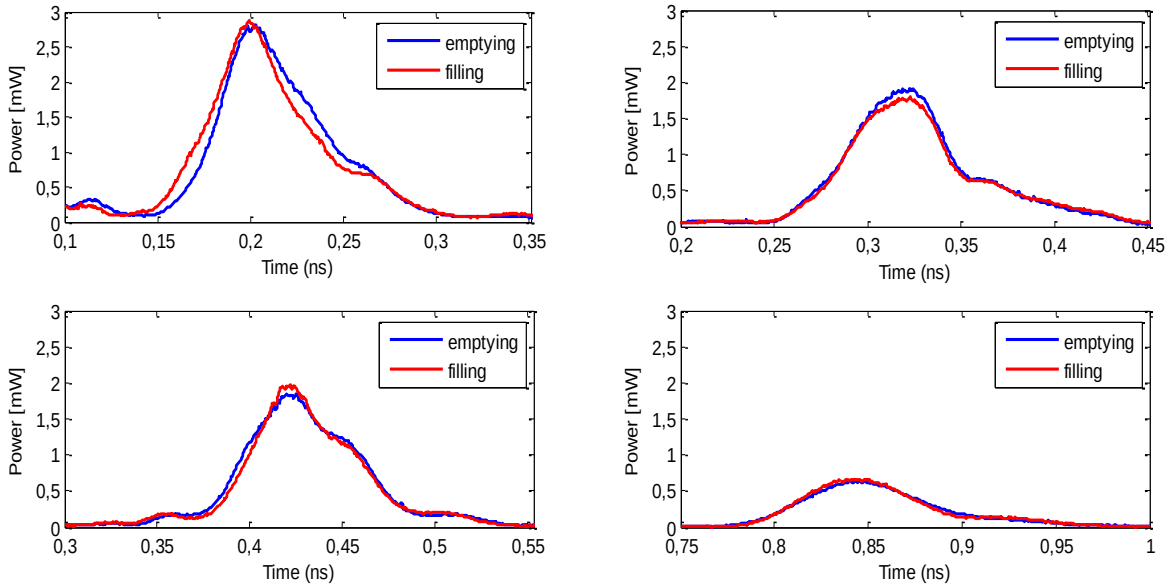

Fig. 14. Measurements of the sensor repeatability obtained by step-emptying and step-filling the container: (top-left) liquid level of 8.27 cm, (top-right) liquid level of 7.07 cm, (bottom-left) liquid level of 6.01 cm, (bottom-right) liquid level of 1.66 cm.

Finally, experimental measurements have been obtained by both step-emptying and step-filling the container in order to show the stability and repeatability of the sensor, as depicted in Fig. 14. As seen, the sensing setup shows a good stability and repeatability.

II.5. *Temperature sensing*

The sensor is also able to determine the temperature of the liquid surrounding the FBG, according to the fact that 1°C shift in temperature corresponds to 10 pm shift in Bragg wavelength. Another set of measurements is obtained by launching into the fiber a continuous wave and scanning the central frequency, when almost 4 cm of the entire length of the FBG is surrounded by the liquid. The spectral responses of the FBG captured by means of an OSA are showed in Fig. 15.

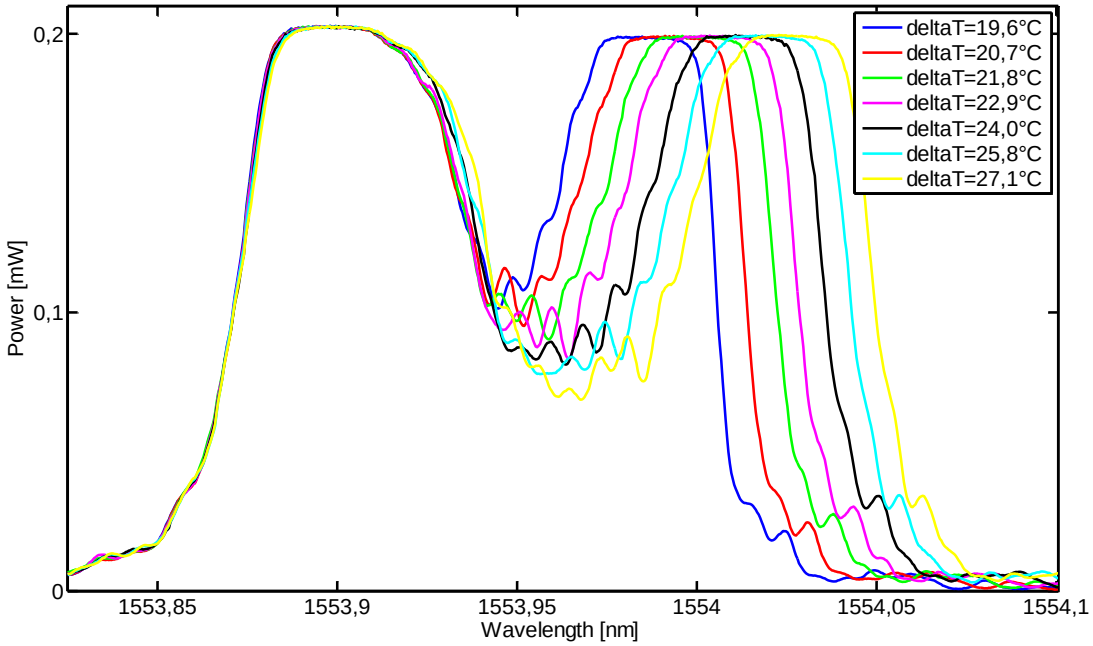

Fig. 15. FBG spectra for different liquid temperature.

In each reflection spectra of the above figure it is possible to distinguish two different component: the first one, fixed at $\lambda_B = 1553.9\ nm$, represents the contribution of the part of the FBG which is not immersed in the liquid, whilst the other component which is moving in wavelength as the temperature changes, is related to the portion of the grating immersed in the liquid. Finally, the sensor is able to detect very high temperature, as the maximum temperature change detectable when CW configuration is used, only depends by the tunability range of the laser. The wider the range, the higher the maximum temperature detectable by the sensor is. On the other hand, the minimum detectable temperature depends on the FWHM bandwidth of the FBG; for this kind of sensing device, it can be estimated that the minimum temperature difference detectable by the sensor is around 7°C.

III. Long FBG sensor interrogation using microwave photonic filtering techniques

As mentioned, FBGs have established their role as key devices in fiber optic-based signal processing systems and applications due to their advantageous characteristics such as simplicity, low insertion loss, polarization independence, low cost and seamless integration in fiber optics systems. In particular, in the context of sensing applications, different methods have been proposed and implemented in order to interrogate the Bragg-frequency distribution along a FBG with the aim of implementing distributed temperature/strain sensors. Some of these salient techniques include optical low-coherence reflectometry (OLCR) [18], optical frequency domain reflectometry (OFDR) [19], synthesis of optical coherence function (SOCF) [20], and time-frequency analysis [21].

In this work, a novel technique to interrogate long FBGs and its potential applications to fiber sensing is proposed and demonstrated. It is specifically dedicated to the situation where one or more spot events must be precisely identified and located, such as hot spots or cracks in structures. The fundamental concept for the proposed interrogation technique is inspired on the operation principle of a discrete time Microwave Photonic (MWP) filter [22, 23], in particular on the information on the delays between the different taps of the filter provided by measuring its radiofrequency transfer function given by the S_{21} parameter. The hot-spot position can be evaluated with a spatial accuracy under 0.5 mm using a modulator and a photo-detector. In the simple configuration proposed, the objective has not been the evaluation of the exact value of temperature or strain, but the detection of its presence and position. However, by opportunely controlling the tunable filter the system is certainly able to provide an estimation of the magnitude under measurement, without using any more devices or additional wavelength-scanned systems. To demonstrate the performance of the proposed technique, firstly, a 10 cm-long strong FBG has been fabricated as a sensing device able to detect one or more hot-spots having different temperatures and located at certain points of the grating. Then, in order to reduce the bandwidth of the devices used in the interrogation system (modulator and photo-detector), a reference arm has been included achieving a correct performance of the quasi-distributed sensor operating with a modest bandwidth of only 1 GHz.

III.1. *Introduction to Microwave Photonics*

Microwave photonics (MWP) [24] is an emerging field that collects together the fields of radio-frequency (RF) engineering and optoelectronics (see Fig. 16). This discipline has attracted great interest over the past 30 years, not only from both the research community but also from the commercial sector, and nowadays it is set to have a bright future. The reason of this choice comes to the fact that it enables the realization of key functionalities in microwave systems that are either complex or even not directly possible in the radio-frequency domain. In addition, MWP creates new opportunities for information and communication (ICT) systems and networks. Indeed,

operations like agility, flexibility, reconfigurability, tunability and wide-band operations are highly desirable features, which are not straightforward to implement by using traditional electronic circuitry; and to date, only MWP approaches have provided promising results in terms of these demanded features.

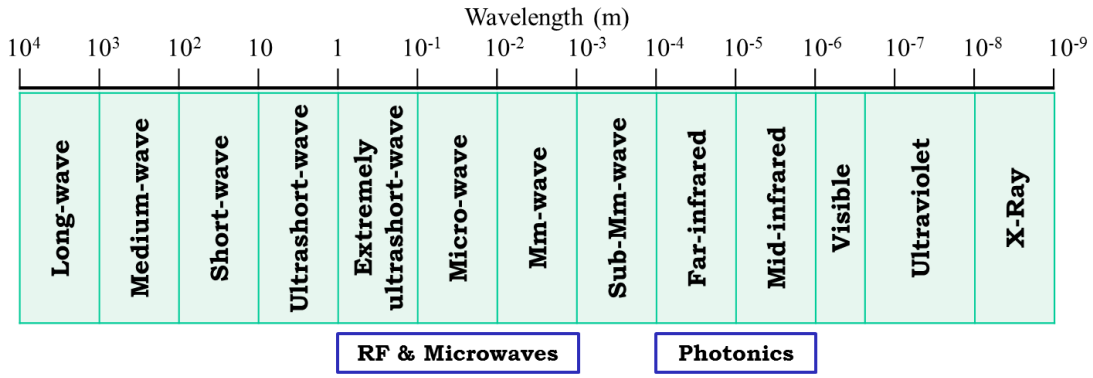

Fig. 16. The electromagnetic spectrum.

Microwave photonics allows the generation, control, processing, transmission and detection of RF, microwave and millimeter-wave signals by means of optical components. This technology enables the use of photonic components and devices for some important practical application, amongst others:

- High purity microwave signal and waveform generation
- Tunable and reconfigurable adaptive filtering
- Optical beam-forming by means of True Time Delay (TTD) and phase shift
- Optoelectronics oscillators
- Optically assisted analogic to digital conversion (ADC)
- Radio over Fiber (ROF) communication systems

Therefore, MWP enables several functions which are difficult or even impossible to carry out with traditional RF technologies, since photonic signal processing can overcome some of the drawbacks caused by the limited bandwidth of the conventional electrical signal processors.

III.2. *Principle of operation*

The setup used to interrogate the long FBG is based on the principle of operation of a MWP filter and is depicted in Fig. 17. The output of a continuous wave (CW) light source is electro-optically modulated with a microwave signal generated. At the output of the electro-optical modulator (EOM) the modulated optical signal is split into N arms. Each arm has a delay-line and an attenuator (or amplifier) in order to provide a delayed and weighted replica of the original signal. These time-delayed and weighted optical signals are combined together and photo-detected. In the

detection process, the different taps can be mixed according to either a coherent or an incoherent basis. In case of incoherent mixing, the tap combination at the photo-detector is insensitive to environmental effects, stable and with a remarkably good repeatable performance. For these reasons, the experimental setup that it is proposed to interrogate the long FBG has been implemented under incoherent operation. The microwave signal is acquired and the electrical frequency response *H(ω)* of such a structure is given by [23]:

$$H(\omega) = \sum_{k=0}^{N} a_k e^{-jk\omega T_k} \tag{14}$$

where $\boldsymbol{\omega}$ is the microwave frequency and a_k is the weight of the k-th replica that is delayed by T_k. When for each value of k, $T_k = T$, Eq. 14 identifies a transfer function with a periodic spectral characteristic; the frequency period is known as *free spectral range* (FSR) and it is inversely proportional to the spacing T between samples [23].

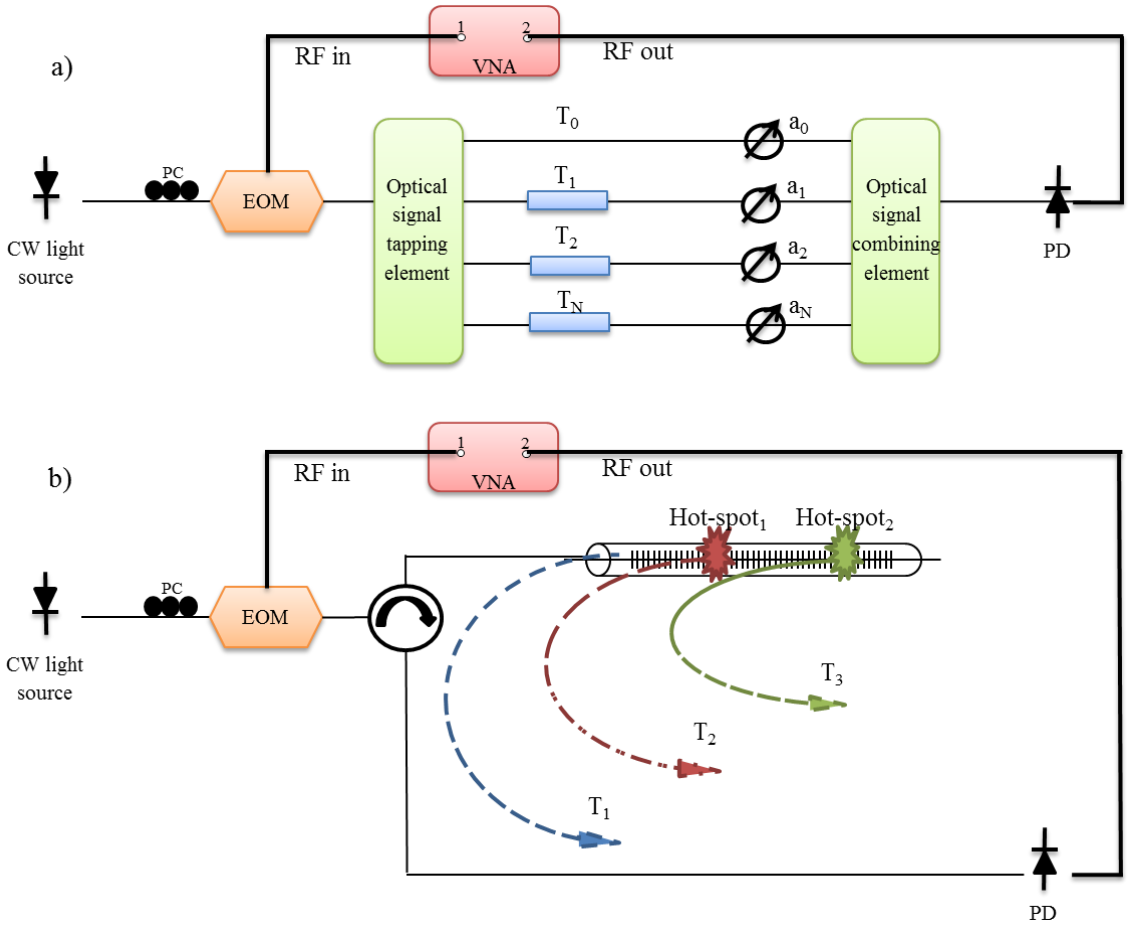

Fig. 17. a) Schematic diagram of an N taps microwave photonic filter. Fig. 17 b). Schematic diagram of the interrogation of the long FBG using MWP techniques.

The proposed sensor produces delayed replicas of the original signal at the input end of the FBG and at each of the hot-spots to be measured [5, 21]. Thus, the response of the FBG sensor is described also in Eq. 14, where the number of taps is equal to the number of hot-spots plus one – the reference reflection normally placed at the entry point of the FBG – and the delays are given by the product of the speed of light within the FBG and the distance between the beginning of the FBG and the location of each hot-spot (see Fig. 17).

The main limitation of this technique arises from the fact that the conditions for *incoherent regime* operation have to be guaranteed. This implies that the minimum delay between two consecutive hot spots, $T = min\{T_{k+1}-T_k\}$ has to verify that $t_c << T$ where t_c, the optical source *coherence time* is given by [25]:

$$t_c = \frac{1}{\pi \Delta f} \tag{15}$$

where Δf is the typical spectral bandwidth of the source. To reduce the value of t_c and to obtain a better range, a broadband source is proposed. The delay between the two consecutive hot-spots is related to the distance L between them by:

$$T = \frac{2n_o L}{c} \tag{16}$$

where n_0 is the refractive index of the fiber and $\boldsymbol{c}$ is the speed of light in vacuum. Therefore, to secure an incoherent regime:

$$L >> \frac{c}{2\pi n_0 \Delta f} = \frac{\lambda^2}{2\pi n_0 \Delta \lambda} \tag{17}$$

where $\Delta f = c\Delta\lambda/\lambda^2$, being $\Delta\lambda$ the source line-width in wavelength units and $\boldsymbol{\lambda}$ the central emission wavelength.

Figures 18a and 18b show the frequency response of a two taps uniform MWP filter and the frequency response of a three taps MWP filters having different spacing between the adjacent samples, respectively. In the first case, it is easy to determine the time-spacing between the two taps; indeed it results to be $T = 1/FSR$. While, in the second case, as the taps of the filter are not equally time-spaced there is not just one FSR and the determination of the time-spacing between the adjacent taps is not as easy as before. However, these separations in time can be evaluated by means of the *inverse Fourier transform* (IFT) of the frequency response of the filter, as will be shown in the next section.

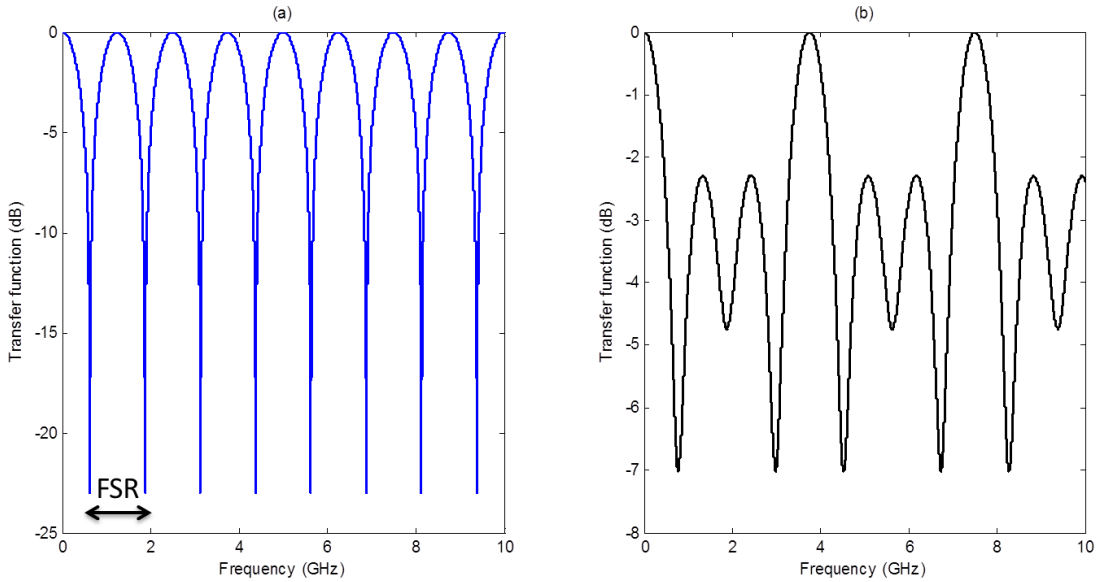

Fig. 18 a). Frequency response of a two taps uniform MWP filter. Fig. 18 b). Frequency response of a three taps MWP filters having different spacing between the adjacent samples.

III.3. *System setup and experimental measurements*

Figure 19 shows the experimental setup used to interrogate a 10 cm-long FBG. A broadband signal provided by a semiconductor optical amplifier (SOA) is filtered by means of a tunable pass-band filter featuring a bandwidth of 0.45 nm centered at the Bragg wavelength of a long FBG. The resonance of the FBG is 1554 nm at room temperature. Using Eq. 15, a time coherence of 5.66-ps for the filtered optical source is obtained, which dictates a smallest time spacing between hot-spots of ~ 50-ps. This implies that the distance between hot-spots should be longer than 5-mm to maintain the conditions of the incoherent regime.

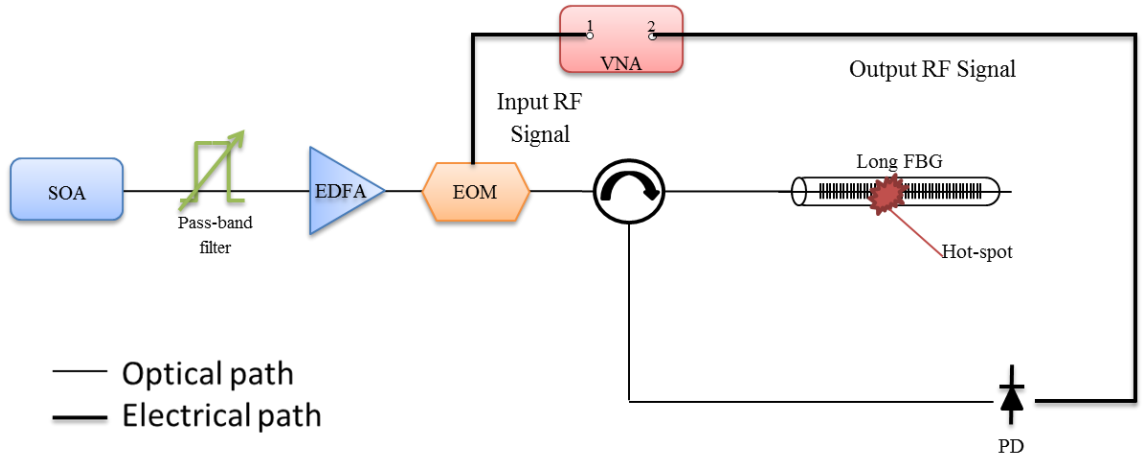

Fig. 19. Experimental setup used to interrogate the 10 cm-long FBG.

The output of the tunable filter is electro-optically modulated with a microwave signal generated by a Vector Network Analyzer (VNA). The microwave signal consists of a radio frequency (RF) tone swept from 10 MHz to 10 GHz. At the output of the EOM, the signal is sent into the FBG through an optical circulator. The signal reflected by the grating is photo-detected. In this way, the frequency response of the waveguide can be analyzed by monitoring the scattering parameter S_{21}, which relates the RF detected signal with the input modulating microwave signal.

Due to the high reflectivity of the FBG, most of the input signal is reflected at the initial section of the FBG [5]. However, a local change of temperature in a hot-spot placed at a certain point along the grating will produce a local Bragg frequency shift. When this occurs, besides the main reflected signal, which is generated at the initial section of the grating, a second reflected signal is produced at the point where the hot-spot is placed. In this way, the presence of a hot-spot results in a two taps MWP filter and it is possible to determine the location of the hot-spot zone by evaluating the FSR of the filter as it is described by Eq. 14.

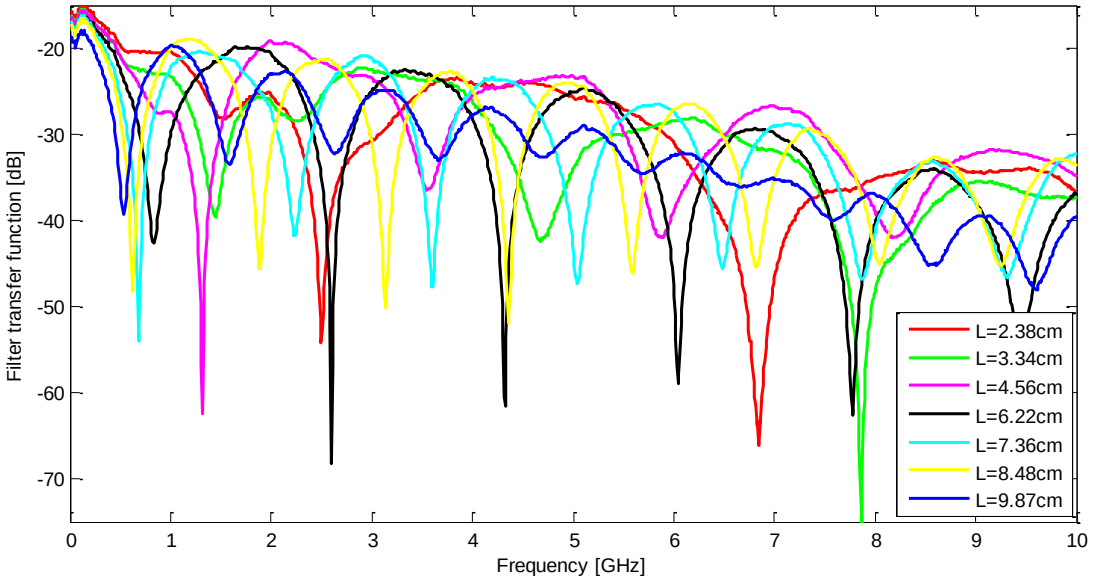

Fig. 20. Frequency response of the two taps filters achieved by placing a hot-spot at a point of the FBG. Inset: position of the hot-spot.

Figure 20 shows the experimental results obtained by moving the hot-spot along the FBG. As expected the recover response is similar to a two tap MWP filter. The FSR has been evaluated with a frequency step of 0.01 MHz, which corresponds to an estimated spatial accuracy under 0.5 mm. The length spacing between the two taps is calculated according to Eq. 16 and from this value the hot-spot position is determined. The inset in Fig. 20 shows the position of the hot-spot.

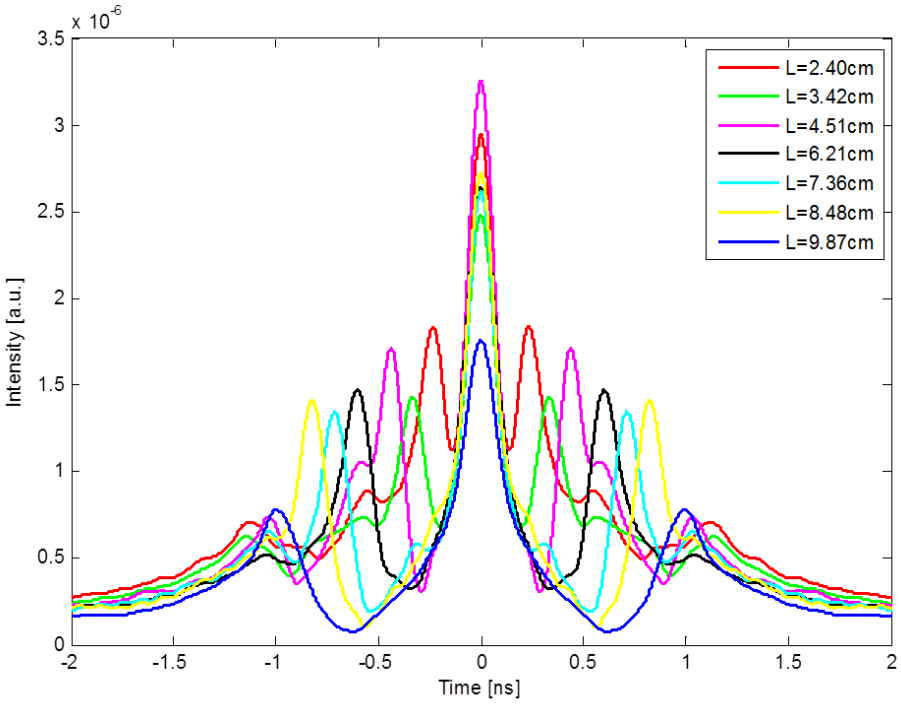

Fig. 21. IFT of the module frequency response of the filters in Fig. 20. Inset: Hot-spot location.

The fiber length spacing between the two taps can be easily evaluated by means of the inverse Fourier transform (IFT) of the graphs displayed in the above figure. Fig. 21 shows the result of the calculation of the IFT of the module frequency response of the filters showed in Fig. 20. The time-difference between the main peak and the pair of secondary peaks represent the time spacing T between the two samples and, once again, the length spacing between the two taps can be calculated by using Eq. 16. The inset in Fig. 21 shows the calculated position of the hot-spot.

When another hot-spot is placed along the grating length, a three taps filter is achieved and a transfer function similar to the one illustrated in Fig. 18b is represented at the monitor of the VNA. Figure 22a shows the response of the sensor when one and two hot-spots are present (two and three taps filters, correspondingly). Since retrieving the delays directly from the transfer function is time consuming, the most efficient approach to calculate the distance between the input end of the FBG and the two hot-spots is simply to take the IFT of the measured S_{21} parameter. Fig. 22b shows the IFT of the amplitude of the transfer function of the three tap filter illustrated in Fig. 22a where two hot-spots are placed along the grating and the IFT of the module of the two taps filter obtained when one of the hot-spots is suppressed.

The time differences between the main peaks and the two pairs of sub-pulses from Fig. 22b (blue curve) represent the time spacing T_1 and T_2 between the beginning of the FBG and the first and second hot-spot, respectively. By using Eq. 16, the distance between the entry point of the grating and the first hot-spot is calculated to be 4.20 cm, while the distance between the grating entry point and the second hot-spot is 7.82 cm.

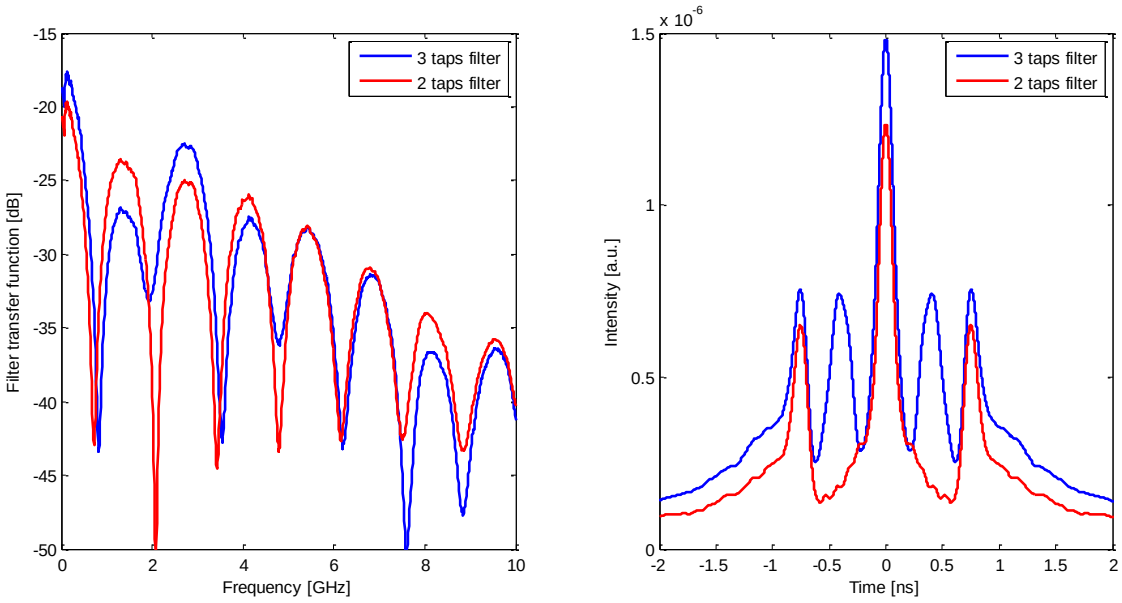

Fig. 22 a). Frequency response of 3 taps and 2 taps filters obtained by placing 2 hot-spots and one hot-spot along the grating, respectively. Fig. 22 b). Inverse Fourier transform of the module of the MWP filters shown in Fig. 22 a).

To alleviate the bandwidth requirements of the modulator and the photo-detector, a variant of the setup is proposed, which is illustrated in Fig. 23. A reference arm is used in this case in order to obtain higher time spacing T between taps, which leads to a shorter FSR, when only one hot-spot is detected. Fig. 24a and Fig. 24b show that the hot-spot position can be evaluated by using a modulator and a photo-detector with a modest bandwidth of less than 1 GHz.

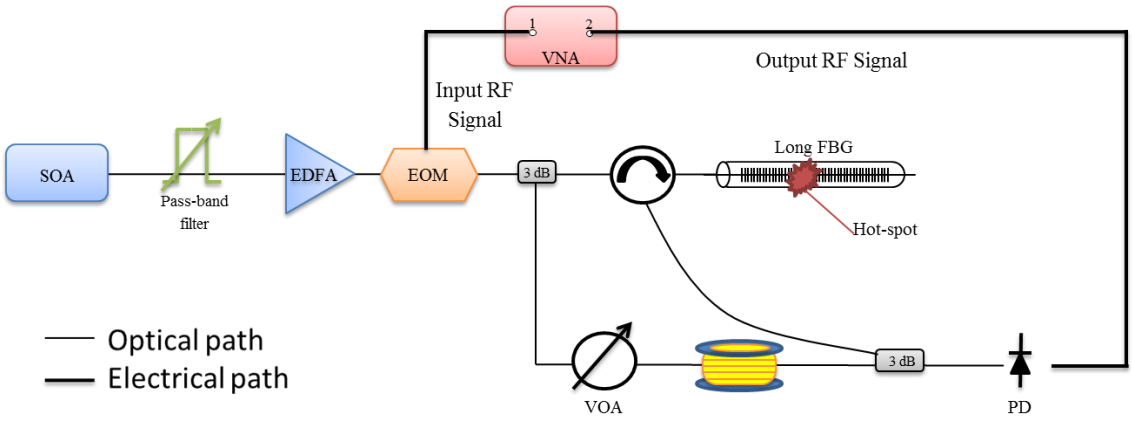

Fig. 23. Experimental setup using a reference arm to obtain higher time spacing between the MWP filter taps.

In this scheme, the signal reflected by the initial section of the grating is mixed at the photo-detector with the signal coming through the reference arm. The reference arm has a Variable

Optical Attenuator (VOA), which is used to control the amplitude of the sample in order to reach, as much as possible, the amplitude of the FBG tap. In this way, the frequency response module of the MWP filter captured by the VNA is improved and better measurements of its FSR are performed. Furthermore, the time spacing between the taps can be controlled by opportunely changing the length of the single mode fiber (SMF) which is placed in the reference arm, in order to achieve higher time spacing, which means a shorter FSR. Therefore, the system proposed is able to recover the signals in a bandwidth lower than 1 GHz that means a less-expensive setup. The blue curve in Fig. 24a and Fig. 24b represents the two tap filter created by the combination of the tap provided by the signal reflected by the FBG and the tap provided by the reference arm.

When a hot-spot is placed along the FBG, another tap is created, which means a three taps MWP filter. In order to simplify the measurement process, a two taps filter is desirable; for this reason, by moving the optical filter, the tap created at the initial section of the FBG is filtered out and, in this way, a two tap MWP filter is achieved (due to the combination of the tap provided by the signal reflected by the hot-spot and the tap provided by the reference arm). The results of this set of measurements are shown in Fig. 24a and 24b. Once again, as has been done for the measurements performed by using the scheme in Fig. 19, the location of the hot-spot in the FBG can be calculated using Eq. 16 with a spatial accuracy of less than 0.5 mm.

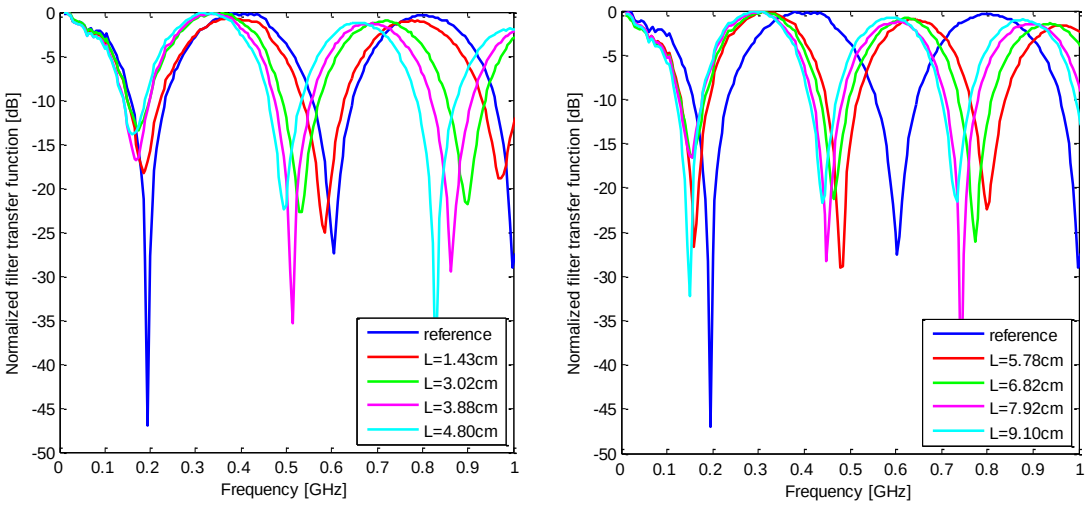

Fig. 24 a) and b). Microwave photonics two taps filters obtained by using a tap provided by a reference arm and a tap provided by a hot-spot located in the long FBG.

III.3 *Microwave photonic filters and inverse Fourier transform*

In the work presented, the inverse Fourier transform results a key mathematical instrument for the calculation of hot-spots location. Indeed, as it was mentioned in the previous section, in case of a single spot event, the measurement can be easily performed by calculating the time spacing between the taps (which is the inverse of the filter FSR) and by using Eq. 16. On the contrary,

when more spot events are located along the sensing FBG, a MWP filter of three or more taps is achieved and the position of each hot-spot must be determined by means of the IFT. In this case, the spatial resolution (i. e. the minimum distance over which two events are not distinguishable), depends on the frequency step of the VNA and on the number of "notches" captured.

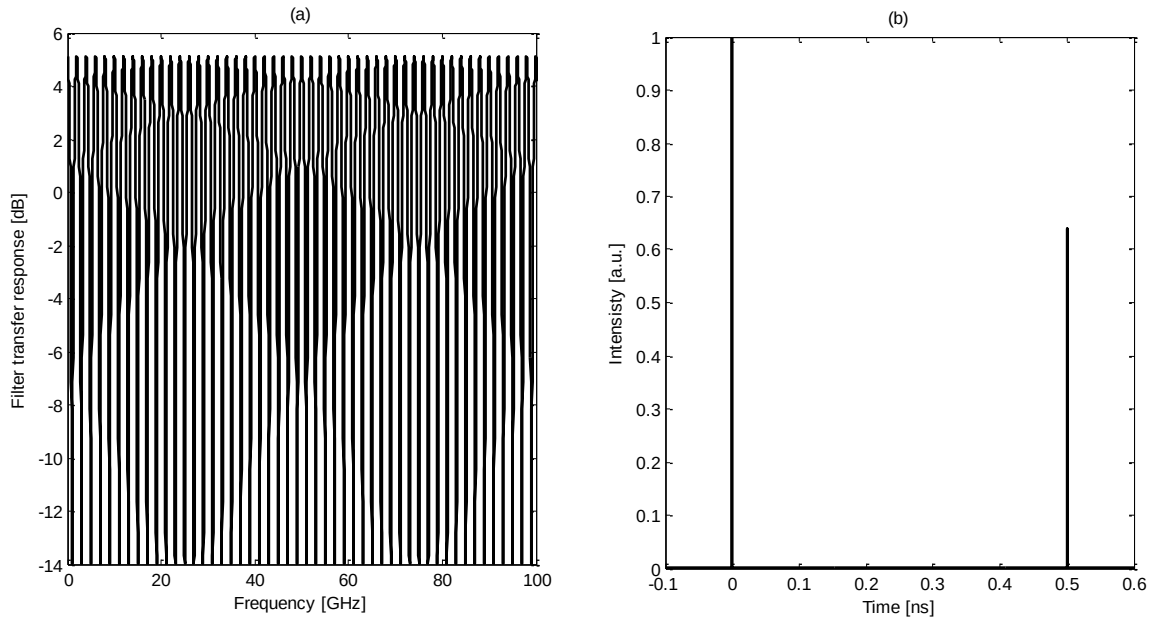

Fig. 25 a). MWP two taps filter with 10.000 nothces. Fig. 25 b). IFT of the filter in Fig. 25a.

The best spatial resolution may be achieved if the device was able to scan infinite frequency values, but obviously, in case of a real instrument, this is not possible. Fig. 25a and Fig. 25b show the spectral response of a two taps MWP filter which presents 10.000 notches in a frequency range of 20 THz, with a time spacing between the two taps of 0.5 ns and the corresponding IFT, respectively. As can be seen, when a very high number of "notches" is captured and processed, the IFT of the filter spectral response presents two *dirac delta* signals, whose time spacing represents the time difference between the two filter taps. In this case, the measurements can be achieved with an ideal infinitesimal spatial resolution.

In practice, it is not possible to reach a quasi-infinite number of notches and these very high values of frequency range. Therefore, the limited bandwidth of the devices and the discrete number of notches leads to a decrease in the spatial resolution, as illustrated in Fig. 26. When the number of the notches and the frequency range is reduced, the pulses corresponding to the IFT of the filter spectral response are enhanced and the spatial resolution is reduced.

To alleviate the problem of the pulse enhancing, a *zero padding* of the filter frequency response before the calculation of the IFT is proposed and the results are depicted in Fig. 27. In this way, although the physical limitation of the setup reduce the spatial resolution of the method, a simple mathematical process, such as the addition of a train of zeros to the frequency waveform captured

by the VNA, allows a “re-shaping” of the pulses corresponding to the IFT of the filter spectral response which leads to an improvement in the spatial resolution.

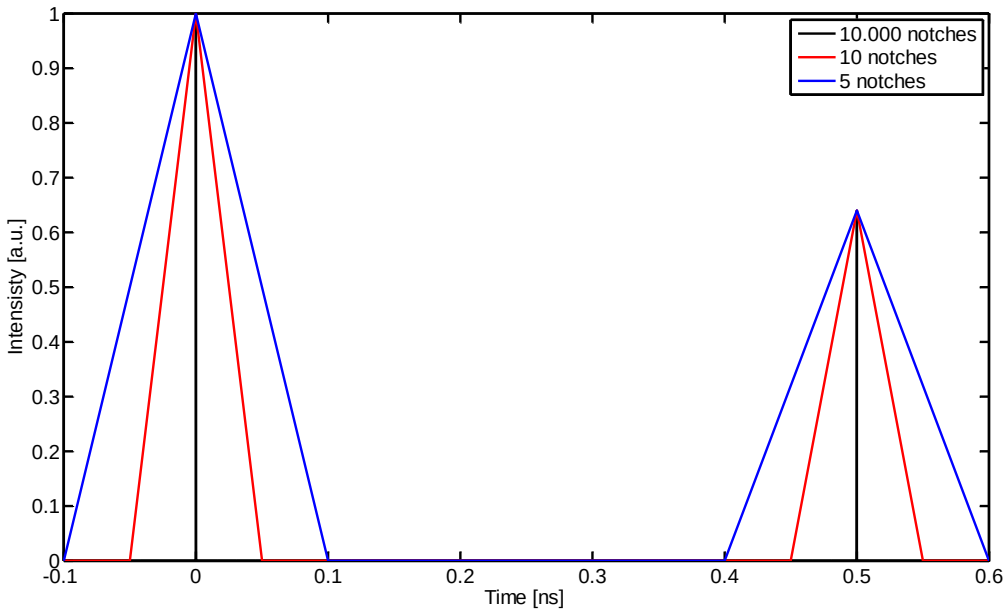

Fig. 26. IFT of different MWP filters varying in number of notches and frequency range.

This theoretical analysis about the IFT employed to the proposed time-discrete microwave photonic filtering technique, allows to estimate a priori the devices bandwidth requirements when a concrete value of the spatial resolution is attempt. In case of 10 GHz frequency range and for 5 notches, by using zero padding a spatial resolution of less than 1 cm is theoretically evaluated.

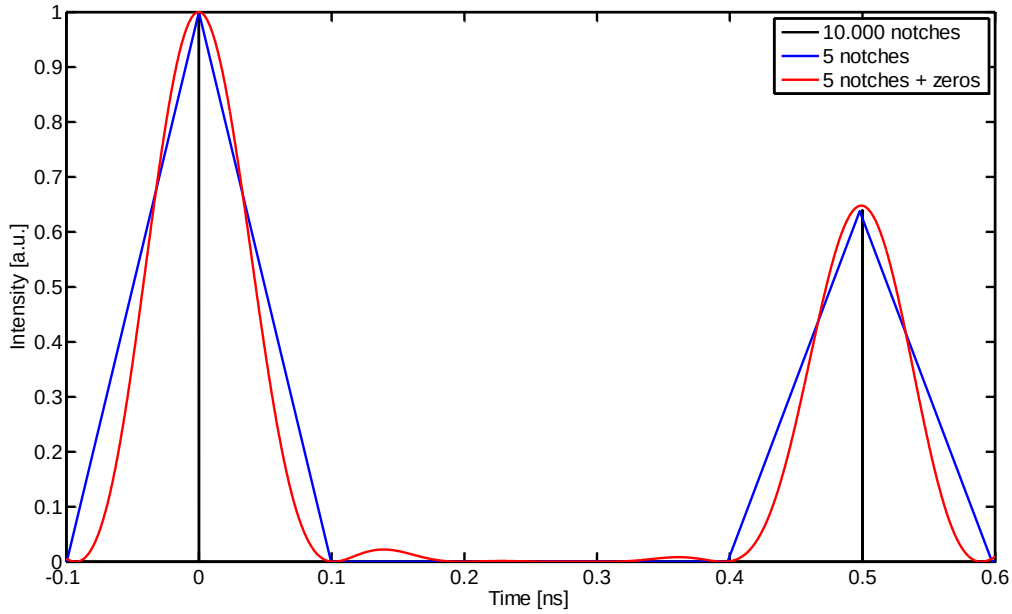

Fig. 27. IFT of different MWP filters varying in number of notches and IFT of a filter frequency with zero padding for improving the spatial resolution.

IV. Conclusions

The work proposed has been focused on the study, design and performance evaluation of fiber Bragg gratings to the aim of realizing distributed sensing devices able to discriminate both liquid level and temperature change. The reason for this choice relays on the fact that FBGs have established their role as key devices in fiber optic-based signal processing systems and applications due to their advantageous characteristics such as simplicity, low insertion loss, polarization independence, low cost and seamless integration in fiber optics systems. Furthermore, FBGs are made of dielectric material and hence non conducting, immune to electromagnetic interference (EMI), chemically inert and spark free.

Nowadays, FBGs are extensively implemented in different kinds of application scenarios such as sensors, filters, switches and for multiplying pulse repetition rates, amongst others. In the context of sensing applications, different methods have been proposed and implemented in order to interrogate the Bragg-frequency distribution along a FBG with the aim of implementing distributed temperature/strain sensors, such as optical low-coherence reflectometry (OLCR), optical frequency domain reflectometry (OFDR), synthesis of optical coherence function (SOCF) and time-frequency analysis.

In chapter 2, a technique for liquid-level and temperature sensors based on a long FBG was presented and experimentally demonstrated. Liquid level sensing is an indispensable requirement in many applications in which monitoring the liquid's volume is necessary, for example in chemical processing, fuel storage and transportation. Electrical liquid-level sensors are widely used in practice, but their applicability, reliability, and safety is compromised if the liquid to be monitored is conductive or corrosive or if the environment is potentially explosive. Moreover, in case of multiple electrical sensors, it is required intensive wiring, and feed-through, unavoidably increasing the system cost and complexity. Optical fiber liquid-level sensors offer better performance under these rigorous conditions because of their advantageous characteristics. The time-frequency analysis of a 10 cm-long FBG and its potential applications for fiber liquid-level sensing have been proposed and experimentally demonstrated. A short optical pulse was coupled into a strong FBG. By monitoring the back-reflected pulse by an oscilloscope a liquid-level sensing is achieved with a spatial resolution of 2 mm, determined by half the incident pulse duration, and with a long measurement range of 10 cm. If a continuous wave is launched into the FBG and the central frequency is scanned, a liquid-temperature sensing is achieved with a minimum temperature variation between air and liquid of 7°C. The proposed technique presents important advantages if compared with others liquid level systems: a simpler configuration, long measurement range, and high spatial resolution.

In chapter 3, a novel technique for interrogating photonic sensors based on long FBGs was presented and experimentally demonstrated, dedicated to detect the presence and the precise

location of several spot events. The measurement system was based on the principle of operation of a microwave photonics filter, in particular on the measurement of the electrical S_{21} parameter that characterizes the filter transfer function. Two different alternatives have been proposed in order to estimate the position of a 5 mm hot-spot along the FBG. In the first one, a simple configuration is employed to interrogate a 10 cm-long FBG in which the frequency of operation has been swept from 10 MHz to 10 GHz. By evaluating the FSR of the resulting MWP filter, the location of a single hot-spot along the long FBG can be detected with a remarkable precision. In the case of two or more hot-spots simultaneously present along the FBG, the fastest method is to derive the corresponding delays by taking the IFT of the measured RF transfer function (S_{21} parameter). In the second configuration, a reference arm has been used in order to achieve higher time spacing between the taps, which means a shorter FSR. In this case, the hot spot position has been evaluated by using a less-expensive setup, which includes a modulator and a photo-detector of only 1 GHz-bandwidth. In both configurations, the location of the hot spot in the sensing FBG was calculated with a 0.5 mm spatial accuracy, depending on the instrumental spatial resolution. Using this simple scheme the magnitude of the hot spots can also be evaluated by opportunely controlling the tunable filter, although this study was not reported here, as it was beyond the scope of this work.

V. Future research

Although the long FBG sensor devices reported in this work have shown capabilities for the discrimination of liquid-level and temperature sensing, the optimization of their performance and demonstration of further applications in discrete-time MWP field will required additional study and research.

In particular, the open research lines include:

- Study the influence of the pulse shape and duration on the spatial resolution and time-frequency response of the grating under test.

- Perform a deep analysis of the temperature sensing system in order to provide an estimation of the measurement accuracy and resolution.

- Find a proper mechanism for the liquid level detection that can be make the proposed system able to the detection of the liquid level even if the temperature change between the liquid and the surrounding ambient is of a few degree or no temperature difference is produced.

- Obtain experimental results for the temperature detection of the spot events presented in the discrete-time microwave photonic techniques. In the simple configuration proposed, the objective has not been the evaluation of the exact value of temperature or strain, but the detection of its presence and position. However, by opportunely controlling the tunable filter, it is certainly able to provide an estimation of the magnitude under measurement, without using any more devices or additional wavelength-scanned systems.

- Perform a deep and exhaustive analysis of the spatial resolution of the measurements achieved by using the MWP filter approach.

- Propose a novel technological platform for the detection of various temperature spot event placed along the gratin, which may present the same temperature.

ACKNOWLEDGEMENTS

The authors wish to acknowledge the financial support of the Infraestructura FEDER UPVOV08-3E-008, FEDER UPVOV10-3E-492 and the Ministerio de Ciencia e Innovación through the project TEC2011-29120-C05-05, the Valencia Government through the Ayuda Complementaria ACOMP/2013/146, European Commission through the COST Action TD1001 "OFSeSa" and the Swiss National Science Foundation through project 200021-134546.

BIBLIOGRAPHY

[1] B. Culshaw, *Optical fiber sensor technologies: Opportunities and perhaps pitfalls*, J. Lightwave Technol. 22, 39-50 (2004).

[2] A. Othonos and K. Kalli, D. Pureur, and A. Mugnier, *Wavelength Filters in Fibre Optics*, Springer, Chap. 5 (2006).

[3] T. Erdogan, *Fiber Grating Spectra*, J. Lightwave Technol. 15, 1277-1294 (1997).

[4] P. S. J. Russell, J. L. Archambault, and L. Reekie, *Fiber gratings*, Physics World, 41-46 (1993).

[5] L. R. Chen, P.W.E. Smith, J.E. Sipe, *Ultrashort pulse reflection from fiber gratings: a numerical investigation*, J. Lightwave Technol. 22, 1503-1551 (1997).

[6] A. Kersey, M. A. Davis, H. J. Patrick, M. Leblanc, K. P. Koo, C.G. Askins, M.A. Putnam, E. J. Friebele, *Fiber grating sensors*, J. Lightwave Technol. 15, 1442-1463 (1997).

[7] S. Khahiq, S. W. James, and R.P. Tatam, *Fiber-optic liquid-level sensor using a long-period grating*, Opt. Lett. 26, 1224–1226 (2001).

[8] B. Yun, N. Chen, and Y. Cui, *Highly sensitive liquid-level sensor based on etched fiber Bragg grating*, IEEE Photon. Technol. Lett. 19, 1747–1749 (2007).

[9] K. R. Sohn and J. H. Shim, *Liquid-level monitoring sensor systems using fiber Bragg grating embedded in cantilever*, Sensors and Actuators A, 248-251 (2009).

[10] T. Guo T, Q. Zhao, Q. Dou, H. Zhang, L. Xue, G. Huang, X. and Dong, *Temperature-insensitive fiber Bragg grating liquid level sensors based on bending cantilever beam*, IEEE Photon. Technol. Lett. 17, 2400–2402 (2005).

[11] E. Antonio-Lopez, J.J. Sanchez-Mondragon, P. LiKamWa, and D. A. May-Arrioja, *Fiber-optic sensor for liquid level measurement*, Opt. Lett. 36, 3425 3427 (2011).

[12] K.P. Chen, B. McMillan, and L. Cashdollar, *Self heated fiber Bragg grating sensors*, Appl. Phys. Lett. 86, 143503 (2005).

[13] F. Pérez-Ocón, M. Rubiño, J.M. Abril, P. Casanova, and J.A. Martínez, *Fiber-optic liquid-level continuous gauge*, Sensors and Actuators A 125, 124-132 (2006).

[14] M. Bottacini, N. Burani, M. Foroni, F. Poli, and S. Selleri, *All-plastic optical-fiber level sensor*, Microwave and Optical Technol. Lett. 46, 520-522 (2005).

[15] M. Lomer, A. Quintela, M. López-Amo, J. Zubia, J.M. López-Higuera, *A quasi-distributed level sensor based on a bent side-polished plastic optical fibre cable*, Meas. Sci. Technol. 18, 2261-2267 (2007).

[16] M. K. Barnoski, M. D. Rourke, S. M. Jensen and R.T. Melville, *Optical time domain reflectometer*, Appl. Opt. 16, 2375-2379 (1997).

[17] N. J. Doran and D. Wood, *Nonlinear-optical loop mirror*, Opt. Lett., vol. 13, 56-58 (1988).

[18] M. Volanthen, H. Geiger, and J. P. Dakin, *Distributed grating sensors using low-coherence reflectometry*, J. Lightwave Technol. 15, 2076-2082 (1997).

[19] E. E. Sanborn, A. K. Sang, E.Wesson, D. E. Wigent III, G. Lucier, *Distributed Fiber Optic Strain Measurement using Rayleigh Scatter in Composite Structures*, Experimental and Applied Mechanism 6, 461-470 (2011).

[20] K. Hotate and K. Kajiwara, *Proposal and experimental verification of Bragg wavelength distribution measurement within a long-length FBG by synthesis of optical coherence function*, Opt. Express 16, 7881-7887 (2008).

[21] J. Sancho, S. Chin, D. Barrera, S. Sales, L. Thévenaz, *Time-frequency analysis of long fiber Bragg gratings with low reflectivity*, Opt. Express 21, 7171-7179 (2013).

[22] J. Capmany, B. Ortega, D. Pastor, S. Sales, *Discrete-time optical processing of microwave signals*, J. Lightwave Technol. 23, 702-723 (2005).

[23] J. Capmany, J. Mora, I. Gasulla, J. Sancho, J. Lloret, and S. Sales, *Microwave Photonic Signal Processing*, J. Lightwave Technol. 31, 571-586 (2013).

[24] S. Iezekiel, *Microwave Photonic:, devices and applications*, Wiley, Chap. 1 (2009).

[25] C.H. Henry, *Theory of the linewdith of semiconductor laser*, IEEE J. Quantum Electron., 18, 259-264, (1982).

ANNEXES

UNIVERSIDAD POLITECNICA DE VALENCIA
iTEAM Instituto de Telecomunicaciones y Aplicaciones Multimedia
OQCG Optical and Quantum Communications Group

OPTICAL AND QUANTUM COMMUNICATIONS GROUP
iTEAM - Edificio 8G - C/ Camino de Vera s/n
46022 - Valencia (Spain) - Tel. +34.96.387.95.80
infogco@gco.upv.es - http://www.gco.upv.es/

Fiber-optic liquid level sensing by using a long fiber Bragg grating.

Amelia Lavinia Ricchiuti

INTRODUCTION

Liquid level sensing is an indispensable requirement in many applications in which monitoring the liquid's volume is indispensable, for example in chemical processing, fuel storage and transportation. Uniform fiber Bragg grating (FBGs) are simple to fabricate and to interrogate. Besides, FBGs can be multiplexed easily for multipoint measurement and fluctuations of the received power do not affect the measurement.
A technique for liquid-level sensors based on a 10 cm long FBG was experimentally demonstrated. The measurement system was based on the measurement of the central frequency distribution of the FBG based on time-frequency domain analysis.

SENSOR DESIGN

A short optical pulse, having duration much shorter than the transit time through the FBG and generated by a laser operating at 1554nm, is launched into a 10-cm long FBG. The resonance of the FBG at room temperature is 1554 nm too and it is mounted in a graduated container.

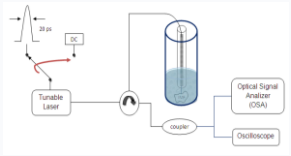

Fig. 1: Experimental layout to interrogate the 10-cm long FBG liquid-level sensor.

During the experiment, the container was filled and emptied with water having temperature higher than the ambient. The reflected pulse was captured with an Optical Signal Analyzer (OSA) and an oscilloscope. When the FBG is partially immersed in the liquid, it can be considered to have two gratings. When the optical pulse is coupled into the FBG, a separation of the reflected pulse in two components, separated by the round-trip propagation time between the two FBGs, is observed. By evaluating the time separation between the two peaks, the liquid level can be detected with 2 mm spatial resolution, which is essentially determined by half the pulse duration.

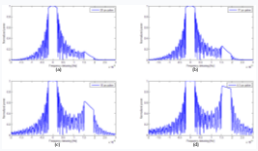

Fig. 2: Product between the grating reflection response of a 10 cm FBG when 4 cm of the grating are immersed in a liquid with temperature 35°C higher than the ambient and different input pulse spectrum: (a) pulse time duration of 20 ps, (b) pulse time duration of 17 ps, (c) pulse time duration of 10 ps, (d) pulse time duration of 4.5 ps.

EXPERIMENT

Experimental measurements have been obtained by step-emptying and step-filling the container in order to show the stability and repeatability of the sensor.

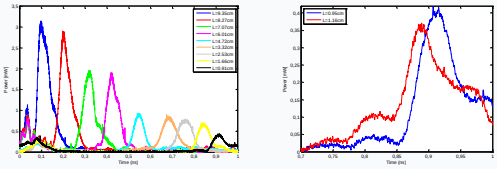

Fig. 3: (Left) Measurements of the reflected pulse time waveform obtained by step-emptying the container. (Right) Sensor spatial resolution.

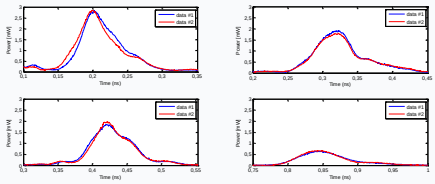

Fig. 4: Measurements of the sensor repeatability obtained by step-emptying and step-filling the container: (top-left) liquid level of 8.27 cm, (top-right) liquid level of 7.07 cm, (bottom-left) liquid level of 6.01 cm, (bottom-right) liquid level of 1.66 cm.

Liquid temperature was measured by launching into the FBG a continuous wave (CW) and by scanning the central frequency, when almost 4-cm of the entire length of the FBG were in the liquid. The spectral response of the FBG is captured by means of an OSA.

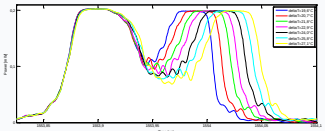

Fig. 5: FBG spectra for different liquid temperature.

As the laser can be moved in 2,5 nm range, the maximum temperature variation detectable by the sensor if CW configuration is used, is almost 200°C.

CONCLUSION

The time-frequency analysis of a 10-cm long FBG and its potential applications for liquid-level sensing have been demonstrated. A short optical pulse was coupled into a strong FBG. By monitoring the back-reflected pulse, the liquid level was detected with a 2 mm spatial resolution and 10 cm long measurement range. When a CW was used, the liquid temperature was determined with a minimum temperature variation between air and liquid of 7,5°C. The proposed technique presents important advantages such as simple configuration, long measurement range, and high spatial resolution.

This work was carried out with the financial support of the Infraestructura FEDER UPVOV08-3E-008, FEDER UPVOV10-3E-492 and the Ministerio de Ciencia e Innovación through the project TEC2011-29120-C05-05.

Fiber-optic liquid-level sensor using a long fiber Bragg grating

Amelia Lavinia Ricchiuti[1], David Barrera[1], Koji Nonaka[2] and Salvador Sales[1]

[1]ITEAM Research Institute, Optical and Quantum Communications Group, Universidad Politécnica de Valencia, Camino de Vera s/n, 46022 Valencia, Spain,
amric1@iteam.upv.es
[2]Kochi University of Technology, Japan

ABSTRACT

A technique for liquid-level sensors based on a long fiber Bragg grating (FBG) is presented and experimentally demonstrated. The measurement system is based on the measurement of the central frequency distribution of the FBG based on time-frequency domain analysis. A short optical pulse is injected into a 10-cm long FBG mounted in a container. The back-reflected pulse is scanned by means of an oscilloscope. When part of the grating is immersed in a liquid having temperature higher than the surrounding ambient, the structure of the uniform grating is distorted and its time-frequency response changes. A spatial resolution of 2 mm, given by the input pulse duration, and a 10-cm long measurement range are achieved. Liquid-temperature sensing has also been implemented by scanning the spectral response of the FBG by means of a CW laser and an OSA.
Keywords: Liquid-level sensor, FBG, high spatial resolution, long measurement range.

1. INTRODUCTION

Liquid level sensing is an indispensable requirement in many applications in which monitoring the liquid's volume is necessary, for example in chemical processing, fuel storage and transportation. Electrical liquid-level sensors are widely used in practice, but their applicability, reliability, and safety is compromised if the liquid to be monitored is conductive or corrosive or if the environment is potentially explosive. Moreover, in case of multiple electrical sensors, it is required intensive wiring, and feed-through, unavoidably increasing the system cost and complexity. Optical fiber liquid-level sensors offer better performance under these rigorous conditions because they are made of dielectric material and thus they are no-conducting, immune to electromagnetic interference, chemically inert and spark free[1]. Different kinds of optical fiber liquid-level sensors have been reported based on: Long-Period Gratings (LPGs)[2], etched Fiber Bragg Gratings (FBGs)[3], FBGs placed in mechanical cantilevers[4-5], High-Birefringence-fiber Loop Mirror (HBFLM)[6], no-core multimode fiber (MMF)[7], arrays of FBGs[8].

In this paper, a technique for fiber-optic liquid-level sensors based on a 10-cm long uniform FBG is proposed and demonstrated. Uniform FBGs are simple to fabricate and to interrogate. Besides, FBGs can be multiplexed easily for multipoint measurement and fluctuations of the received the power do not affect the measurement. A short optical pulse having duration much shorter than the transit time through the FBG has been employed. If a portion of the FBG is immersed in a liquid having a temperature different to the surrounding ambient, the structure of the uniform grating is distorted and its response will change. By captured and monitored the reflected pulse by means of an oscilloscope, it is possible to implement a liquid-level sensor with high resolution and long measurement range based on a simple layout. The temperature of the liquid can also be measured.

2. SENSOR SYSTEM DESIGN AND EXPERIMENT

A schematic diagram of the proposed Fiber Bragg Grating liquid-level sensor is shown in Fig. 1. A short optical pulse, having duration of 20 ps and generated by a laser operating at 1554nm, is launched into a 10-cm long FBG. The resonance of the FBG is 1554 nm at room temperature. The FBG is mounted inside a graduated container. During the experiment, the container is filled (or emptied) with water having temperature higher than the surrounding ambient. Finally, the reflected pulse is captured and monitored by using an Optical Signal Analyzer (OSA) and an oscilloscope. The measurement system is based on the measurement of the central frequency distribution of the FBG based on time-frequency domain analysis.

When the short optical pulse is launched into the FBG, as the grating is strong, the incident pulse is almost completely reflected in the initial section of the grating[9].

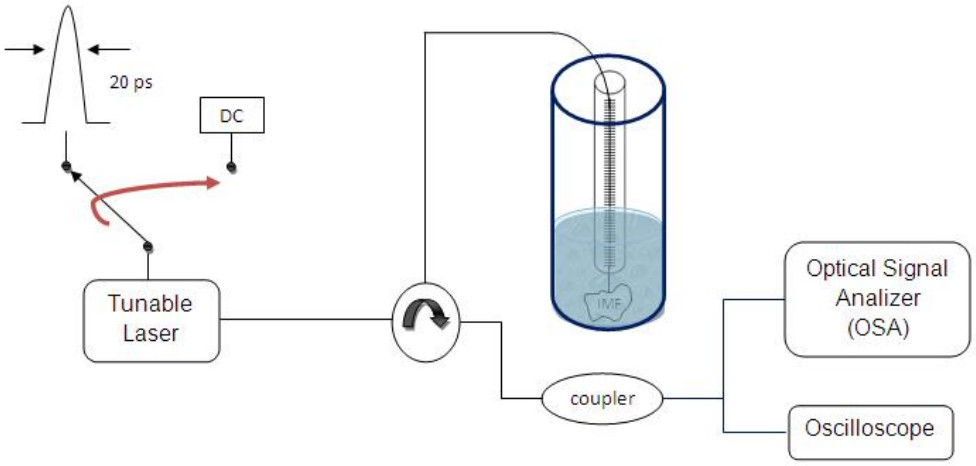

Fig. 1: Experimental layout to interrogate the 10-cm long FBG liquid-level sensor.

If the FBG is partially immersed within the liquid having temperature higher than the surrounding ambient, the structure of the section of the grating immersed will change. Indeed, it can be considered to have two separate gratings; the first one centered at the Bragg wavelength of the original FBG and the other one centered at a new Bragg wavelength. In this case, when the input optical pulse is coupled into the FBG, a separation of the reflected pulse into two distinct components can be observed; a main reflection pulse will be reflected in the initial section of the first FBG, and a transient sub-pulse will be reflected in the initial section of the second FBG (i. e. the portion immersed in the liquid). The main reflection pulse and the sub-pulse are separated in time by the round-trip propagation time between the two different gratings. By evaluating the time-separation between the two peaks, the liquid level can be detected with high spatial resolution. Indeed, as the pulse is always reflected at the beginning of each one of the FBGs, the spatial resolution of this technique is essentially determined by half the pulse duration, such as Optical Time Domain Reflectometry (OTDR) technique. As the optical pulse has duration of 20 ps, the spatial resolution of this system is around 2 mm.

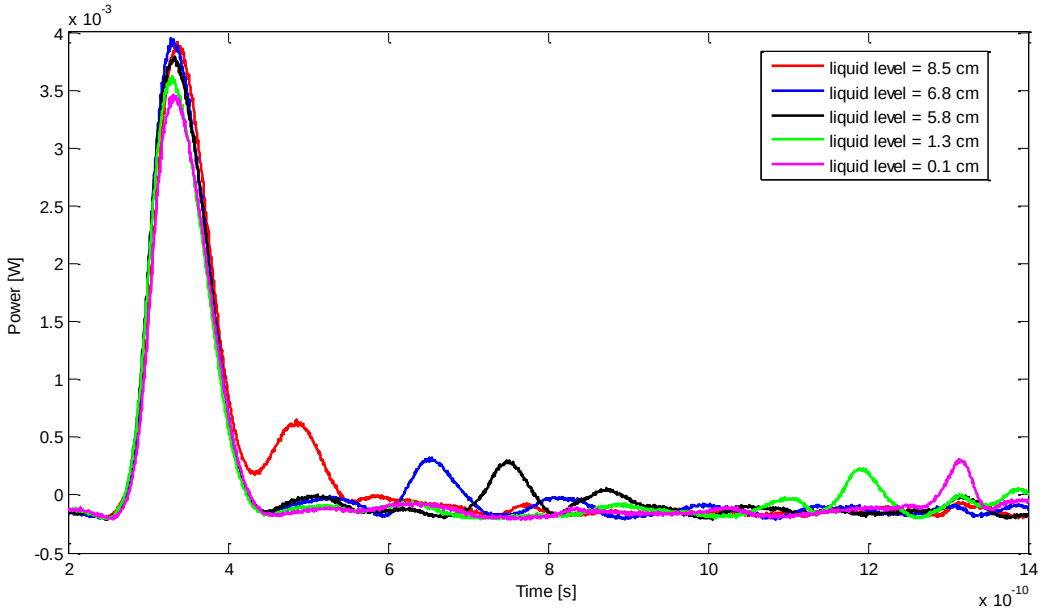

Fig. 2: Measurements of the reflected pulse time waveform obtained by step-emptying the container.

Fig. 2 shows a set of experimental measurements of the reflected pulse time waveform with 2 mm spatial resolution obtained by step-emptying the container. The values of the liquid level can be measured by means

of the time difference between the first back-reflected pulse and the second one. The nominal FBG spectrum is measured under CW illumination giving a FWHM spectral width of 11.25 GHz, while the spectral width of the 20 ps Gaussian pulse is calculated, by means the Time-Bandwidth Product, as FWHM ≈ 0.441/20 ps, i.e. FWHM ≈ 22 GHz. As the FWHM of the incident pulse is almost the double of the FWHM of the FBG, when a change in the liquid level occurs and provokes a change in the FBG spectrum, the main reflection peak, is still completely captured by the Gaussian pulse and then its amplitude remains quite constant, while the shifted secondary peak, is not totally captured thus its amplitude is considerably lower.

In order to evaluate the influence of the time-duration of the optical pulse in this technique, numerical simulations have been implemented. Fig. 3 illustrates the product between the input pulse spectrum and the grating reflection response. We have assumed a grating reflection response of a 10-cm FBG with FWHM ≈ 11 GHz. Then, we simulated that 4 cm of the grating are immersed in a liquid having temperature 35°C higher than the surrounding ambient. Finally we multiplied the FBG spectrum with four different input pulse spectra, varying in temporal duration.

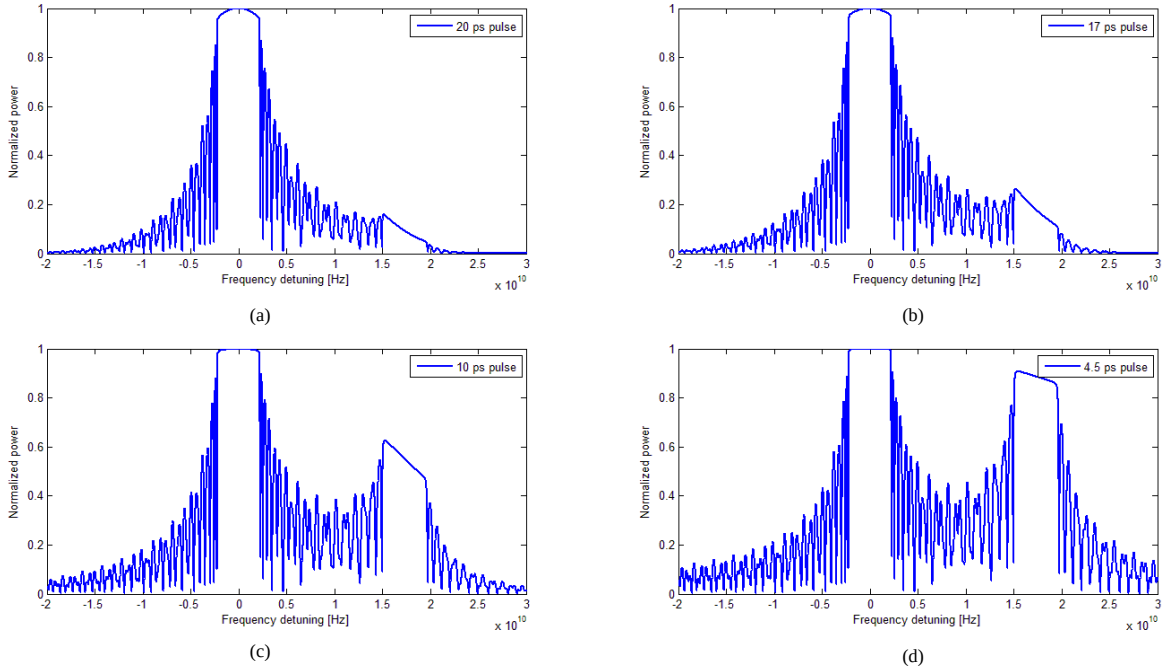

Fig. 3. Product between the grating reflection response of a 10-cm FBG with FWHM ≈ 11 GHz when 4-cm of the grating are immersed in a liquid having temperature 35°C higher than the surrounding ambient and different input pulse spectrum: (a) optical pulse having time duration of 20 ps, (b) optical pulse having time duration of 17 ps, (c) optical pulse having time duration of 10 ps, (d) optical pulse having time duration of 4.5 ps.

By analyzing these numerical simulations, it can be seen that using an optical input pulse of 20 ps, the maximum temperature variation detectable by the sensor is almost 35°C, as showed in Fig. 3(a). Nevertheless, if the time duration of the input pulse is reduced, i.e. the spectral response is enhanced, temperature variation higher than 35°C can also be measured.

The sensor is also able to determine the temperature of the liquid surrounding the FBG, according to the fact that 1°C shift in temperature corresponds to 10 pm shift in Bragg wavelength. Another set of measurements is obtained by launching into the fiber a continuous wave and scanning the central frequency, when almost 4-cm of the entire length of the FBG are surrounding by the liquid. The spectral responses of the FBG captured by means of an OSA are showed in Fig. 4(a). The blue curve represents the FBG spectrum when the container is totally empty. The green and red curves represents the two peaks resonances when a portion of the container is filled with water at a temperature higher than the air, 15°C and 25°C respectively. As the temperature of the liquid can be determined starting by the second peak position shift, as can be seen in the Fig. 4(b), the minimum temperature variation that the sensor is capable of estimate is of 10°C.

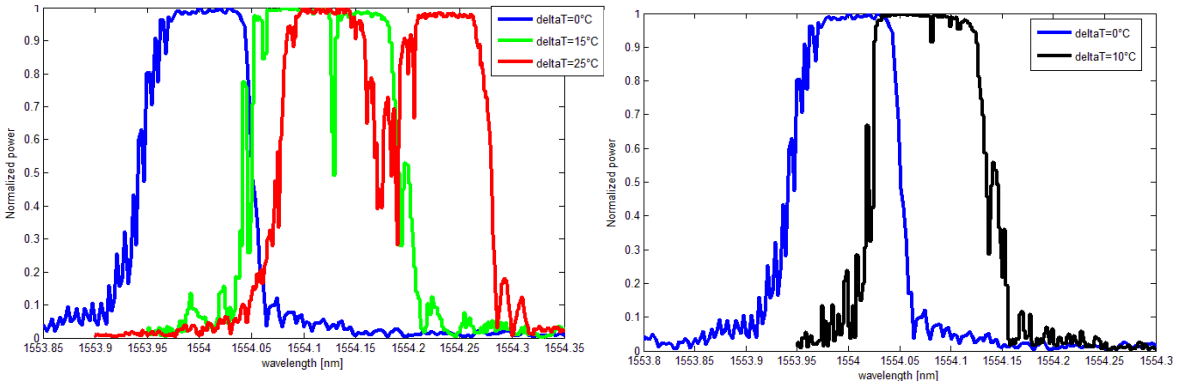

(a) (b)

Fig. 4: FBG spectra for different liquid temperature.

3. CONCLUSION

The time-frequency analysis of a 10-cm long FBG and its potential applications for fiber liquid-level sensing have been proposed and experimentally demonstrated. A short optical pulse was coupled into a strong FBG. By monitored the back-reflected pulse by an oscilloscope a liquid-level sensing is achieved with a spatial resolution of 2 mm, determined by half the incident pulse duration, and with a long measurement range of 10 cm. If a continuous wave is launched into the FBG and the central frequency is scanned, a liquid-temperature sensing is achieved with a minimum temperature variation between air and liquid of 10°C. The proposed technique presents important advantages if compared with others liquid level systems: a simpler configuration, long measurement range, and high spatial resolution.

ACKNOWLEDGMENT
The authors wish to acknowledge the financial support of the Infraestructura FEDER UPVOV08-3E-008, FEDER UPVOV10-3E-492 and the Ministerio de Ciencia e Innovación through the project TEC2011-29120-C05-05.

REFERENCES

[1] Culshaw B., “Optical fiber sensor technologies: Opportunities and perhaps pitfalls”, J Lightwave Technol 22, 39-50 (2004)
[2] Khahiq S., James S. W., and Tatam R. P., “Fiber-optic liquid-level sensor using a long-period grating,” Opt. Lett. 26, 1224–1226 (2001).
[3] Yun B., Chen N., and Cui Y., “Highly sensitive liquid-level sensor based on etched fiber Bragg grating”, IEEE Photon. Technol. Lett. 19, 1747–1749 (2007).
[4] Sohn K. R. and Shim J. H., "Liquid-level monitoring sensor systems using fiber Bragg grating embedded in cantilever", Sensors and Actuators A, 248-251 (2009).
[5] Guo T., Zhao Q., Dou Q., Zhang H., Xue L., Huang G., and Dong X., “Temperature-insensitive fiber Bragg grating liquid level sensors based on bending cantilever beam” IEEE Photon. Technol. Lett. 17, 2400–2402 (2005).
[6] Dong B., Zhao Q., Feng L., Guo T., Xue L., Dong S., and Gu H., “Liquid-level sensor with a high-birefringence-fiber loop mirror”, Appl. Opt. 45, 7767–7771 (2006).
[7] Antonio-Lopez E., Sanchez-Mondragon J. J., LiKam Wa P., and May-Arrioja D. A., “Fiber-optic sensor for liquid level measurement”, Opt. Lett. 36, 3425 3427 (2011).
[8] Chen K. P., McMillan B., and Cashdollar L., “Self heated fiber Bragg grating sensors”, Appl. Phys. Lett. 86, 143503 (2005).
[9] Chen L. R., Smith P. W. E., Sipe J. E., “Ultrashort pulse reflection from fiber gratings: a numerical investigation”, J Lightwave Technol 22, 1503-1551 (1997).

Long fiber Bragg grating sensor interrogation using discrete-time microwave photonic filtering techniques

Amelia Lavinia Ricchiuti[1], David Barrera[1], Salvador Sales[1], Luc Thevenaz[2] and José Capmany[1]

[1]*I3TEAM Research Institute, Universidad Politécnica de Valencia, Camino de Vera s/n, 46022 Valencia, Spain*
[2]*Ecole Polytechnique Fédérale de Lausanne, Institute of Electrical Engineering, SCI-STI-LT Station 11, 1015 Lausanne, Switzerland*
[*]*email*

Abstract: A novel technique for interrogating photonic sensors based on long fiber Bragg gratings (FBGs) is presented and experimentally demonstrated, dedicated to detect the presence and the precise location of several spot events. The principle of operation is based on a technique used to analyze microwave photonics (MWP) filters. The long FBGs are used as quasi-distributed sensors. Several hot-spots can be detected along the FBG with a spatial resolution under 0.5 mm using a modulator and a photo-detector (PD) with a modest bandwidth of less than 1 GHz.

OCIS codes: (060.3735) Fiber Bragg gratings; (060.2370) Fiber optics sensors; (230.1480) Bragg reflectors;

References and links

1. B. Culshaw, "Optical fiber sensor technologies: Opportunities and perhaps pitfalls", J. Lightwave Technol. **22**, 39-50 (2004).
2. A.D. Kersey, M. A. Davis, H. J. Patrick, M. LeBlanc, K. P. Koo, C. G. Askins, M. A. Putnam, and E. J. Friebele, "Fiber Grating Sensors," J. Lightwave Technol. **15**(8), 1442-1463 (1997).
3. S. Y. Li, N. Q. Ngo, S. C. Tjin, P. Shum, and J. Zhang, "Thermally tunable narrow-bandpass filter based on linearly chirped fiber Bragg grating", Opt. Lett. **29**(1), 29-31 (2004).
4. H. Uno, A. Kojima, A. Shibano, O. Mikami, "Optical wavelength switch using strain-controlled fiber Bragg gratings," ICOSN '99, Proc. SPIE **3740** (1999).
5. J. Azaña and M. A. Muriel, "Temporal self-imaging effects: theory and application for multiplying pulse repetition rates", IEEE J. Sel. Top. Quantum Electron., **7**, 728 – 744 (2001).
6. M. Volanthen, H. Geiger, and J. P. Dakin, "Distributed grating sensors using low-coherence reflectometry," J. Lightwave Technol. **15**(11), 2076-2082 (1997).
7. E. E. Sanborn, A. K. Sang, E.Wesson, D. E. Wigent III, G. Lucier, "Distributed Fiber Optic Strain Measurement using Rayleigh Scatter in Composite Structures," Experimental and Applied Mechanism **6**, 461-470 (2011).
8. K. Hotate and K. Kajiwara, "Proposal and experimental verification of Bragg wavelength distribution measurement within a long-length FBG by synthesis of optical coherence function," Opt. Express **16**(11), 7881-7887 (2008).
9. J. Sancho, S. Chin, D. Barrera, S. Sales, L. Thévenaz, "Time-frequency analysis of long fiber Bragg gratings with low reflectivity", Opt. Express **21**(6), 7171-7179 (2013).
10. J. Capmany, B. Ortega, D. Pastor, S. Sales, "Discrete-time optical processing of microwave signals", J. Lightwave Technol. **23**, 702-723 (2005).
11. J. Capmany, J. Mora, I. Gasulla, J. Sancho, J. Lloret, and S. Sales, "Microwave Photonic Signal Processing," J. Lightwave Technol. 31, 571-586 (2013)
12. A. V. Oppenheim, R. W. Schafer, J. R. Buck, "Discrete Time Signal Processing", Prentice Hall, Englewood Cliffs, USA (1996).
13. L. R. Chen, S. D. Benjamin, P. W. E. Smith, and J. E. Sipe, "Ultrashort pulse reflection from fiber gratings: a numerical investigation," J. Lightwave Technol. **15**(8), 1503-1512 (1997).
14. C.H. Henry, 'Theory of the linewdith of semiconductor lasers', IEEE J. Quantum Electron., **18**, 259-264, (1982).

1. Introduction

FBGs have established their role as key devices in fiber optic-based signal processing systems and applications due to their advantageous characteristics such as simplicity, low insertion loss, polarization independence, low cost and seamless integration in fiber optics systems. Furthermore, FBGs are made of dielectric material and hence non conducting,

immune to electromagnetic interference (EMI), chemically inert and spark free [1]. For these reasons, FBGs have been extensively implemented in different kinds of application scenarios such as sensors [2], filters [3], switches [4] and for multiplying pulse repetition rates [5], amongst others. In the context of sensing applications, different methods have been proposed and implemented in order to interrogate the Bragg-frequency distribution along a FBG with the aim of implementing distributed temperature/strain sensors. Some of these salient techniques include optical low-coherence reflectometry (OLCR) [6], optical frequency domain reflectometry (OFDR) [7], synthesis of optical coherence function (SOCF) [8], and time-frequency analysis [9].

In this work, a novel technique to interrogate long FBGs and its potential applications to fiber sensing is proposed and demonstrated. It is specifically dedicated to the situation where one or more spot events must be precisely identified and located, such as hot-spots or cracks in structures. The fundamental concept for the proposed interrogation technique is inspired on the operation principle of a discrete time Microwave Photonic (MWP) filter [10, 11], in particular on the information on the delays between the different taps of the filter provided by measuring its radiofrequency transfer function given by the S_{21} parameter. The hot-spot position can be evaluated with a spatial accuracy under 0.5 mm using a modulator and a photo-detector. In the simple configuration proposed, the objective has not been the evaluation of the exact value of temperature or strain, but the detection of its presence and position. However, by opportunely controlling the tunable filter of our system, it is certainly able to provide an estimation of the magnitude under measurement, without using any more devices or additional wavelength-scanned systems. To demonstrate the performance of the proposed technique, firstly, a 10 cm-long strong FBG has been fabricated as a sensing device able to detect one or more hot-spots having different temperatures and located at certain points of the grating. Then, in order to reduce the bandwidth of the devices used in the interrogation system (modulator and photo-detector), a reference arm has been included achieving a correct performance of the quasi-distributed sensor operating with a modest bandwidth of only 1 GHz.

2. Principle of operation

The setup used to interrogate the long FBG is based on the principle of operation of a MWP filter and is depicted in Fig. 1. The output of a continuous wave (CW) light source is electro-optically modulated with a microwave signal generated. At the output of the electro-optical modulator (EOM) the modulated optical signal is split into N arms. Each arm has a delay-line and an attenuator (or amplifier) in order to provide a delayed and weighted replica of the original signal. These time-delayed and weighted optical signals are combined together and photo-detected. In the detection process, the different taps can be mixed according to either a coherent or an incoherent basis. In case of incoherent mixing, the tap combination at the photo-detector is insensitive to environmental effects, stable and with a remarkably good repeatable performance. For these reasons, the experimental setup that it is proposed to interrogate the long FBG has been implemented under incoherent operation. The microwave signal is acquired and the electrical frequency response $H(\omega)$ of such a structure is given by [11]:

$$H(\omega) = \sum_{k=0}^{N} a_k e^{-ik\omega T_k} \tag{1}$$

where ω is the microwave frequency and a_k is the weight of the k-th replica that is delayed by T_k. When $T_k = T,\ \forall k$ Eq. (1) identifies a transfer function with a periodic spectral characteristic; the frequency period is known as *free spectral range* (FSR) and it is inversely proportional to the spacing T between samples [11].

The proposed sensor produces delayed replicas of the original signal at the input end of the FBG and at each of the hot-spots to be measured [9, 13]. Thus, the response of the FBG sensor is described also by Eq. (1), where the number of taps is equal to the number of hot- spots plus one – the reference reflection normally placed at the entry point of the FBG – and the delays are given by the product of the speed of light within the FBG and

the distance between the beginning of the FBG and the location of each hot-spot (see Fig. 1).

The main limitation of this technique arises from the fact that the conditions for incoherent regime operation have to be guaranteed. This implies that the minimum delay between two consecutive hot-spots, $T = \min\{T_{k+1} - T_k\}$ has to verify that $t_c << T$ where t_c, the optical source coherence time is given by [14]:

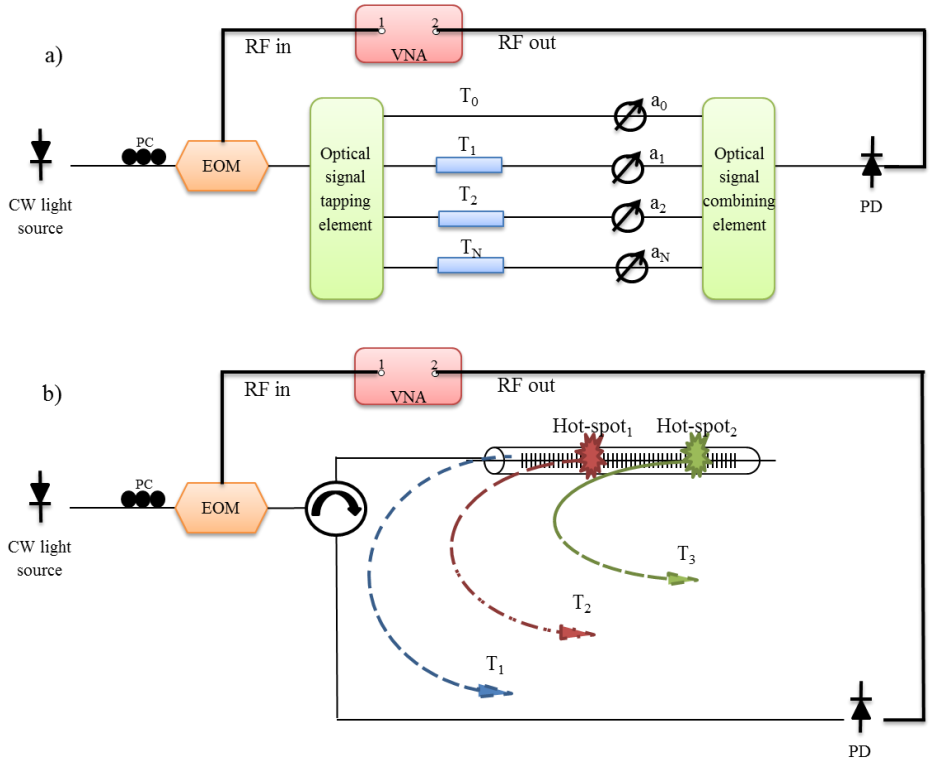

Fig. 1. a) Schematic diagram of an N taps microwave photonic filter. b) Schematic diagram of the interrogation of the long FBG using microwave photonic techniques.

$$t_c = \frac{1}{\pi \Delta f} \tag{2}$$

Here Δf is the typical spectral bandwidth of the source. To reduce the value of t_c and to obtain a better range, a broadband source is proposed. The delay between the two consecutive hot-spots is related to the distance L between them by:

$$T = \frac{2n_o L}{c} \tag{3}$$

where n_0 is the refractive index of the fiber and c is the speed of light in vacuum. Therefore, to secure an incoherent regime:

$$L >> \frac{c}{2\pi n_o \Delta f} = \frac{\lambda^2}{2\pi n_o \Delta \lambda} \tag{4}$$

where $\Delta f = c\Delta\lambda/\lambda^2$ being $\Delta\lambda$ the source linewidth in wavelength units and λ the central emission wavelength.

3. Setup and experimental measurements

Fig. 2 shows the experimental setup used to interrogate a 10 cm-long FBG. A broadband signal provided by a semiconductor optical amplifier (SOA) is filtered by means of a

tunable pass-band filter featuring a bandwidth of 0.45 nm centered at the Bragg wavelength of a long FBG. The resonance of the FBG is 1554 nm at room temperature. Using Eq. (2), a time coherence of 5.66 ps for the filtered optical source is obtained, which dictates a smallest time spacing between hot-spots of ~ 50 ps. This implies that the distance between hot-spots should be longer than 5 mm to maintain the conditions of the incoherent regime.

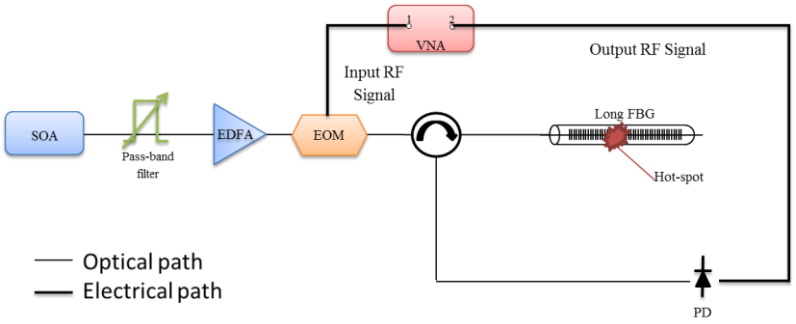

Fig. 2. Experimental setup used to interrogate the 10-cm long strong FBG.

The output of the tunable filter is electro-optically modulated with a microwave signal generated by a Vector Network Analyzer (VNA). The microwave signal consists of a radio frequency (RF) tone swept from 10 MHz to 10 GHz. At the output of the EOM, the signal is sent into the FBG through an optical circulator. The signal reflected by the grating is photo-detected. In this way, the frequency response of the waveguide can be analyzed by monitoring the scattering parameter S_{21}, which relates the RF detected signal to the input modulating microwave signal.

Due to the high reflectivity of the FBG, most of the input signal is reflected at the initial section of the FBG [13]. However, a local change of temperature in a hot-spot placed at a certain point along the grating will produce a local Bragg frequency shift. When this occurs, besides the main reflected signal, which is generated at the initial section of the grating, a second reflected signal is produced at the point where the hot-spot is placed. In this way, the presence of a hot-spot results in a two tap MWP and it is possible to determine the location of the hot-spot zone by evaluating the FSR of the filter as it is described by Eq. (1).

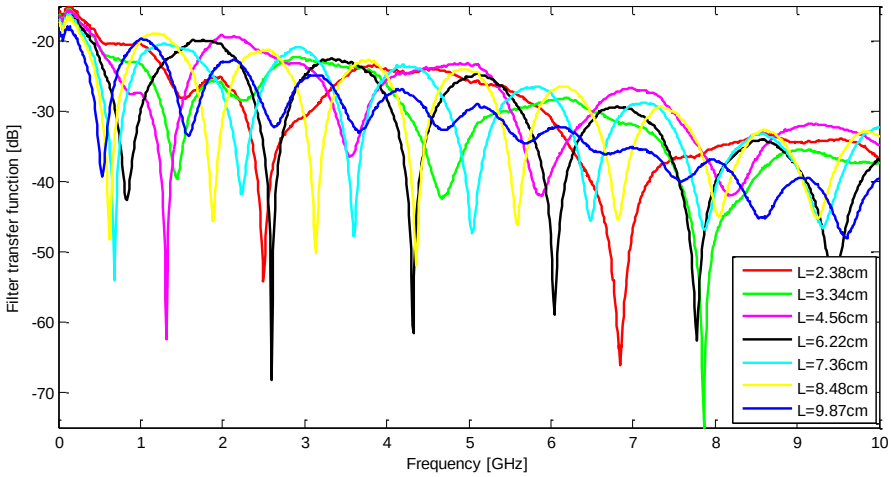

Fig. 3. Frequency response of the two taps filters achieved by placing a hot-spot at a point of the FBG. Inset: position of the hot-spot.

Fig. 3 shows the experimental results obtained by moving the hot-spot along the FBG. As expected the recovered response is similar to a two tap MWP filter. The FSR has been evaluated with a frequency step of 0.01 MHz, which corresponds to an estimated spatial

accuracy under 0.5 mm. The length spacing between the two taps is calculated according to the Eq. (3) and form this value the hot-spot position is determined. The inset shows the position of the hot-spot.

Fig. 4(a) shows the response of the sensor when one and two hot-spots are present (two and three taps, correspondingly). Since retrieving the delays directly from the transfer function is time consuming, the most efficient approach to calculate the distance between the input end of the FBG and the two hot-spots is simply to take the Inverse Fourier Transform (IFT) of the measured S_{21} parameter. Fig. 4(b) shows the IFT of the transfer function of the three tap filter illustrated in Fig. 4(a) where two hot-spots are placed along the grating and the IFT of the module of the two taps filter obtained when one of the hot-spots is suppressed.

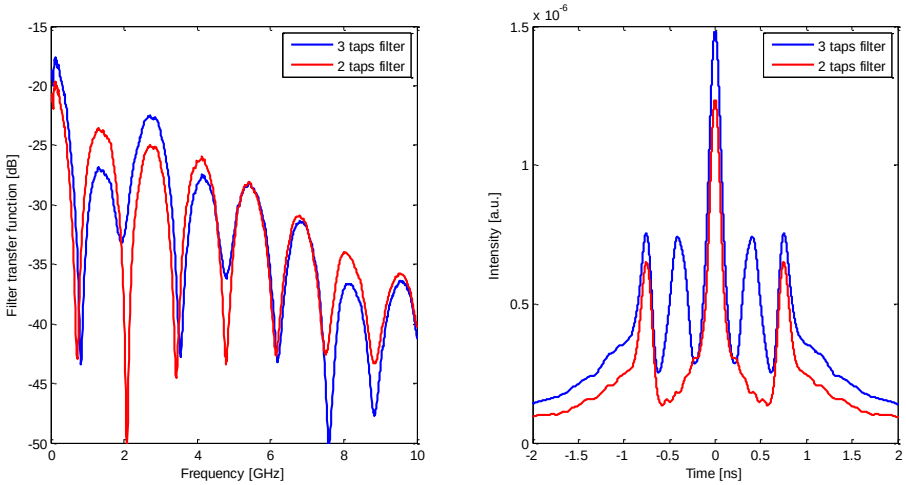

Fig. 4. a) Frequency response of 3 taps and 2 taps filters obtained by placing 2 hot-spots and one hot-spot along the grating, respectively. b) Inverse Fourier transform of the module of the MWP filters shown in Fig. 4(a).

The time differences between the main peaks and the two pairs of sub-pulses from Fig. 4(b) (blue curve) represent the time spacing T_1 and T_2 between the beginning of the FBG and the first and second hot-spot, respectively. By using Eq. (3), the distance between the entry point of the grating and the first hot-spot is calculated to be 4.20 cm, while the distance between the grating entry point and the second hot-spot is 7.82 cm.

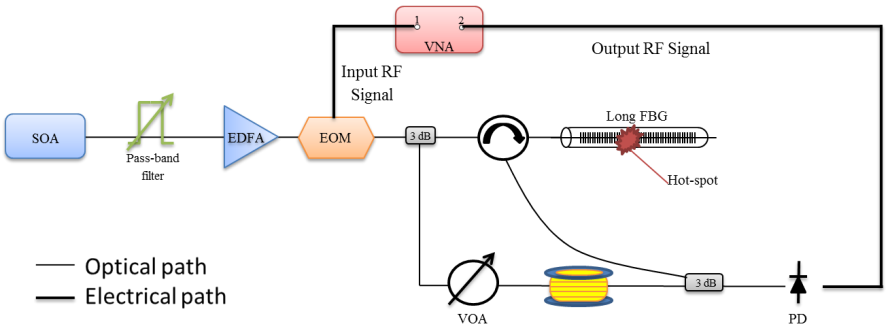

Fig. 5. Experimental setup using a reference arm to obtain higher time spacing between the MWP filter taps.

To alleviate the bandwidth requirements of the modulator and the photo-detector, a variant of the setup is proposed, which is illustrated in Fig. 5. A reference arm is used in this case in order to obtain higher time spacing *T* between taps, which leads to a shorter FSR, when only one hot-spot is detected. Fig. 6(a) and Fig. 6(b) show that the hot-spot position can be evaluated by using a modulator and a photo-detector with a modest bandwidth of less than 1 GHz. Once again the location of the hot-spot in the FBG can be calculated using Eq.(3) with a spatial accuracy of less than 0.5 mm.

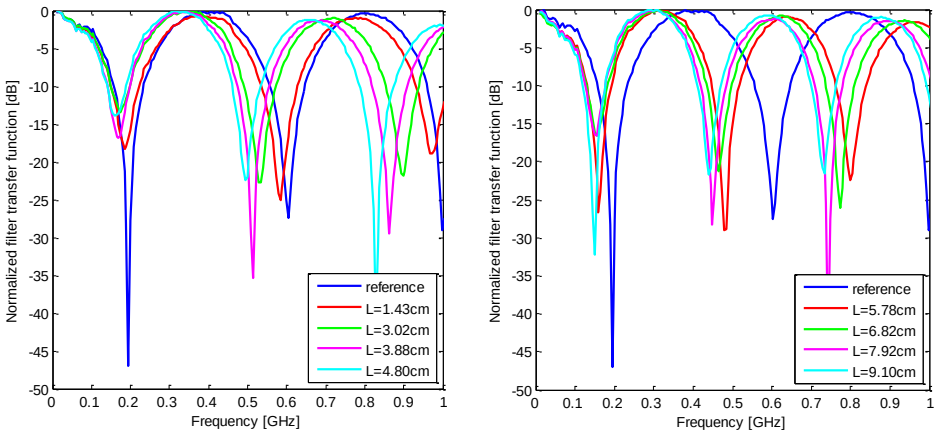

Fig. 6. a) and b) Microwave photonics two taps filters obtained by using a tap provided by a reference arm and a tap provided by a hot-spot located in the long FBG. Inset: position of the hot-spot.

4. Conclusions

In this work, we have proposed and experimentally demonstrated a novel technique for estimating the position and number of hot-spots along a FBG sensor. The measurement system is based on the principle of operation of a microwave photonics filter, in particular on the measurement of the electrical S_{21} parameter that characterizes the filter transfer function. Two different alternatives have been proposed in order to estimate the position of a 5 mm hot-spot along the FBG. In the first one, a simple configuration is employed to interrogate a 10 cm-long FBG in which the frequency of operation has been swept from 10 MHz to 10 GHz. By evaluating the FSR of the resulting MWP filter, the location of a single hot-spot along the long FBG can be detected with a remarkable precision. In the case of two or more hot-spots simultaneously present along the FBG, the fastest method is to derive the corresponding delays by taking the IFT of the measured RF transfer function (S_{21} parameter). In the second configuration, a reference arm has been used in order to achieve higher time spacing between the taps, which means a shorter FSR. In this case, the hot spot position has been evaluated by using a less-expensive setup, which includes a modulator and a photo-detector of only 1 GHz-bandwidth. In both configurations, the location of the hot-spot in the sensing FBG was calculated with a 0.5 mm spatial accuracy, depending on the instrumental spatial resolution, fixed by the instrumental frequency resolution that can be potentially further improved using a higher range instrument. Using this simple scheme the magnitude of the hot-spots can also be evaluated by opportunely controlling the tunable filter, which is a complementary research under study going beyond the scope of this paper.

Acknowledgements

The authors wish to acknowledge the financial support of the Infraestructura FEDER UPVOV08-3E-008, FEDER UPVOV10-3E-492, the Spanish MCINN through the projects TEC2011-29120-C05-05 and TEC2011-29120-C05-01, the Valencia Government through the Ayuda Complementaria ACOMP/2013/146, European Commission through the COST Action TD1001 “OFSeSa” and the Swiss National Science Foundation through project 200021-134546.

Submitted to *Optics Express* on 6th September 2013.